Composite Structures 396 (2026) 120812

Contents lists available at ScienceDirect

Composite Structures

journal homepage: www.elsevier.com/locate/compstruct

An ESL–HSDT finite element model with a variational exponential thickness function for thermo-mechanical analysis of composite plates

Aleksandar Radaković [a,*], Dragan Čukanović [b], Gordana Bogdanović [c], Petar Knežević [b], Strahinja Milenković [a], Aleksandar Nešović [a]

[a] University of Kragujevac, Institute for Information Technologies Kragujevac, Liceja Kneževine Srbije 1A, 34000 Kragujevac, Serbia
[b] University of Priština in Kosovska Mitrovica, Faculty of Technical Sciences, Knjaza Miloša 7, 38220 Kosovska Mitrovica, Serbia
[c] University of Kragujevac, Faculty of Engineering, Sestre Janjić 6, 34000 Kragujevac, Serbia

ARTICLE INFO

Keywords:
Higher-order shear deformation theory
Equivalent single-layer model
Laminated composite plates
Thermo-mechanical bending
Finite element method
Thickness shape function
Variational approach
Transverse shear effects

ABSTRACT

This paper presents a novel finite element formulation for the thermo-mechanical bending analysis of orthotropic and laminated composite plates, developed within the framework of an equivalent single-layer higher-order shear deformation theory (ESL–HSDT). In contrast to conventional higher-order models, which rely on pre-defined polynomial approximations through the thickness and thereby limit the physical accuracy of shear representation, the proposed approach introduces an exponential thickness shape function whose governing parameter is determined through a variational criterion, reducing the arbitrariness associated with predefined through-thickness functions and providing a physically grounded representation of transverse shear deformation.

By directly linking the kinematic assumptions to the through-thickness distribution of transverse shear deformation, the formulation ensures a smooth and mechanically consistent prediction of deformation and stress distributions without the need for shear correction factors. The model is implemented using a four-node quadrilateral finite element with seven degrees of freedom per node, thus maintaining high computational efficiency while preserving higher-order kinematic accuracy.

The accuracy and robustness of the proposed formulation are validated through a series of benchmark problems involving orthotropic and laminated plates subjected to both uniform and spatially varying thermal loads, as well as mechanical loading. The results show good agreement with reference solutions from the literature and three-dimensional elasticity theory, with small deviations for global response quantities and larger discrepancies observed only for local transverse shear stresses, which is consistent with the expected behaviour of ESL formulations.

Compared to classical and layerwise approaches, the proposed model achieves a comparable level of accuracy while significantly reducing computational cost, demonstrating that the adopted thickness function effectively captures interlaminar shear effects within an equivalent single-layer framework.

The developed formulation provides a robust and computationally efficient tool for the analysis of composite plates under coupled thermo-mechanical loading and establishes a physically motivated basis for the further development of advanced through-thickness modeling strategies.

1. Introduction

The analysis of laminated composite and sandwich plates continues to represent a challenging problem, primarily because an accurate description of deformation and stress distributions through the thickness is essential for the reliable prediction of structural response and damage mechanisms. This issue becomes particularly important under thermo-mechanical loading, where the mismatch of thermal expansion coefficients between adjacent layers, together with temperature gradients through the thickness, induces interlaminar stresses, bending, and complex three-dimensional stress states, as demonstrated in exact, analytical, and refined layerwise formulations [1–3]. Such effects may promote damage initiation, including delamination, which further underlines the need for reliable through-thickness modeling. In addition,

* Corresponding author.
E-mail addresses: aradakovic@uni.kg.ac.rs (A. Radaković), dragan.cukanovic@pr.ac.rs (D. Čukanović), gocab@kg.ac.rs (G. Bogdanović), petar.knezevic@pr.ac.rs (P. Knežević), strahinja.milenkovic@kg.ac.rs (S. Milenković), aca.nesovic@kg.ac.rs (A. Nešović).

https://doi.org/10.1016/j.compstruct.2026.120812
Received 17 April 2026; Received in revised form 18 June 2026; Accepted 25 August 2026
Available online 28 August 2026

three-dimensional elasticity solutions have consistently confirmed the inherently three-dimensional nature of stress fields in laminated structures [4,5].

The differences between classical and refined plate theories, including CLT, FSDT, and higher-order formulations, are well established in the literature [6–13]. However, within refined equivalent-single-layer descriptions, a substantial part of the differences in predicting both global and local response is strongly influenced by the adopted through-thickness kinematic assumption. In particular, studies addressing shear correction factors, warping functions, and various higher-order and non-polynomial formulations have demonstrated that different thickness functions introduced within the same theoretical framework may lead to noticeable variations in displacements, transverse shear stresses, and thermoelastic response [8,14–23]. This sensitivity indicates that the through-thickness kinematic description represents one of the governing modeling parameters, rather than a secondary assumption.

To improve the representation of transverse shear effects, a wide range of non-polynomial through-thickness functions has been proposed, including trigonometric, hyperbolic, exponential, and related mixed forms [14–23]. These formulations are generally constructed to satisfy traction-free boundary conditions at the top and bottom surfaces and to eliminate the need for shear correction factors, while often providing improved accuracy compared with lower-order theories.

Recent studies have also explored stress-continuous, zig-zag, and enhanced higher-order formulations as alternative approaches for improving the representation of transverse stress fields and satisfying traction-free surface conditions in laminated and sandwich structures [24–26].

Nevertheless, in most existing approaches, the thickness function is prescribed a priori. Consequently, the resulting solution remains dependent on the assumed through-thickness distribution, which limits the physical generality and robustness of the formulation.

An additional challenge concerns numerical implementation. Although high-er-order theories can provide improved stress prediction, their finite element realization may introduce increased formulation complexity, particularly in displacement-based approaches, as discussed in comprehensive reviews and comparative assessments of refined plate theories [11–13,27–29]. Therefore, theoretical refinement alone does not necessarily guarantee computational efficiency in standard finite element environments.

Accordingly, considerable effort has been devoted to developing formulations that preserve the accuracy of higher-order theories while remaining compatible with C^o-continuous finite element implementations and a limited number of unknowns. In this context, several refined finite element and numerical formulations have been proposed for laminated composite plates, demonstrating that accurate shear-deformable analysis can be achieved without resorting to C^1-continuous elements [30–36]. A representative example is the C^o formulation reported for thermoelastic analysis of laminated composite and sandwich plates, where refined kinematics is successfully combined with computational efficiency [30]. However, even in such approaches, the through-thickness shape function is still predefined, and the fundamental issue of kinematic selection remains open.

On the other hand, layerwise and quasi-three-dimensional approaches provide a more explicit description of displacement fields across individual layers and are capable of capturing interlaminar stresses with high accuracy when compared to three-dimensional elasticity solutions [23,36–42]. Owing to this higher fidelity, they are frequently employed as high-fidelity reference models in detailed thermo-mechanical analyses of laminated and sandwich structures. Their main limitation is the increased computational cost, since the number of generalized variables grows with the number of layers and with the enrichment of the kinematic field. In addition, several studies have shown that transverse normal deformation may play a non-negligible role in thick laminates and in problems involving pronounced thermal gradients [3,22,43], which further complicates the formulation of accurate but efficient plate models.

It should be noted that, as with other equivalent single-layer (ESL) formulations, the accuracy of the proposed model may be reduced for sandwich structures with a very soft core and large stiffness contrasts between the facesheets and the core. In such cases, local through-thickness deformation mechanisms and interlaminar effects may become more significant, and layerwise, zig-zag, or three-dimensional formulations may provide a more detailed representation of the structural response. Consequently, the present formulation is primarily intended for laminated composite plates and structural configurations for which the underlying assumptions of ESL theories remain appropriate.

Taken together, the available literature indicates that current developments are not simply directed toward increasing the polynomial order of approximation, but to-ward defining a through-thickness kinematic description that is both physically meaningful and computationally efficient. In particular, it remains challenging to simultaneously achieve: (i) a through-thickness description supported by a physically or variationally justified criterion, (ii) reliable prediction of transverse shear and inter-laminar stresses, (iii) numerical efficiency compatible with C^o finite element implementation, and (iv) stable accuracy under thermo-mechanical loading.

Motivated by these considerations, the present work proposes a new ESL–HSDT finite element formulation in which the through-thickness shape function is not prescribed in advance, but determined through a variational criterion associated with the through-thickness distribution of transverse shear deformation.

It should be emphasized that the novelty of the present approach does not lie in the adoption of an exponential through-thickness function itself, since exponential HSDT functions have been reported previously in the literature. Rather, the distinguishing feature of the proposed formulation is the variational determination of its governing parameter, which reduces the dependence of the model on a priori prescribed shape-function parameters.

In this way, the adopted kinematics is directly linked to the corresponding through-thickness distribution of deformation energy. The resulting exponential-type function with an adaptive parameter enables a smooth and physically consistent representation of transverse shear effects while reducing the model dependency associated with predefined shape functions. The formulation is implemented within a C^o finite element framework with seven degrees of freedom per node, thereby combining computational efficiency with high predictive capability.

Despite the advantages of the proposed ESL–HSDT formulation, several assumptions and limitations should be acknowledged. As an equivalent single-layer model, the formulation is primarily intended for the accurate prediction of global structural response, while local interlaminar effects can only be represented approximately. Consequently, its accuracy may deteriorate for sandwich structures with highly compliant cores or for problems in which strongly localized through-thickness stress fields play a dominant role. Furthermore, as an equivalent single-layer formulation, the proposed model employs a single continuous through-thickness function to represent the higher-order kinematic contribution. Consequently, displacement-slope discontinuities that may arise at material interfaces are smoothed rather than represented explicitly, unlike in layerwise or zig-zag theories. This limitation may primarily affect the local accuracy of stress predictions in the immediate vicinity of layer interfaces. Nevertheless, compared with layerwise and three-dimensional formulations, the present approach offers a significantly lower computational cost while retaining a physically consistent representation of transverse shear deformation through a variationally determined thickness function.

It is also worth noting that recent developments in computational mechanics have introduced energy-based and physics-informed frameworks, such as the Deep Energy Method (DEM) [45] and its neural-operator extension Variational Neural Operator (VINO) [44], for the solution of variational boundary-value problems. These approaches primarily address the numerical solution stage, whereas the contribution of the present work concerns the formulation stage, namely the development of an improved ESL–HSDT kinematic description based on a variationally determined through-thickness function. The integration of the proposed formulation within such emerging computational frameworks represents an interesting direction for future research.

In the present study, all material, geometric, and loading parameters are treated deterministically; the extension of the proposed formulation toward uncertainty quantification and variance-based sensitivity analysis is therefore left as a subject of future work.

2. Theoretical Formulation

Within higher-order shear deformation theories (HSDT), the choice of the through-thickness distribution function represents a key element of the formulation, as it directly governs the distribution of transverse shear deformation and the corresponding distribution of energy across the plate thickness. As discussed in the previous section, the differences between existing models do not primarily arise from the theoretical framework itself, but from the manner in which this distribution is defined.

In most existing approaches, the through-thickness shape function is assumed a priori, without an explicit physical or variational basis, thereby implicitly imposing energy distribution within the model. Such an approach leads to model-dependent predictions and limits the robustness of the formulation, particularly under thermo-mechanical conditions where the distribution of shear effects plays a critical role.

Existing higher-order plate theories have employed exponential through-thickness functions in various forms. In such formulations, both the functional form and the associated parameters are generally prescribed a priori. In contrast, the present formulation retains an exponential representation but determines its governing parameter through a variational procedure, thereby reducing the arbitrariness associated with the selection of thickness shape functions.

2.1. Kinematic assumptions and displacement field

Within the adopted HSDT framework, a laminated or sandwich plate of total thickness is considered in a Cartesian coordinate system, with the mid-surface defined by $z = 0$, while the top and bottom surfaces are located at $z = \pm h/2$. The layers are assumed to be perfectly bonded, each layer is linearly elastic and orthotropic, and small deformations are considered.

The displacement field of an arbitrary point in the plate is described in terms of the mid-surface displacements and additional generalized kinematic variables describing higher-order variation through the plate thickness. Accordingly, it can be written in the general form as

$$\begin{aligned} u(x,y,z) &= u_0(x,y) + \sum_{I=1}^{2} U^I(x,y)\Phi^I(z), \\ v(x,y,z) &= v_0(x,y) + \sum_{I=1}^{2} V^I(x,y)\Phi^I(z), \\ w(x,y,z) &= w_0(x,y), \end{aligned} \tag{1}$$

where u_0, v_0, w_0 denote the mid-surface displacement components of the plate, while $U^I(x,y)$ and $V^I(x,y)$ represent generalized kinematic variables describing the through-thickness variation of in-plane displacements. The functions $\Phi^I(z)$ denote the adopted through-thickness shape functions. In the proposed formulation, two through-thickness shape functions are adopted

$$\Phi^1(z) = z, \Phi^2(z) = F(z) \tag{2}$$

which leads to the explicit form of the displacement field

$$\begin{aligned} u(x,y,z) &= u_0(x,y) + z\phi_x(x,y) + F(z)\psi_x(x,y) \\ v(x,y,z) &= v_0(x,y) + z\phi_y(x,y) + F(z)\psi_y(x,y) \\ w(x,y,z) &= w_0(x,y) \end{aligned} \tag{3}$$

Here, ϕ_x and ϕ_γ denote rotational variables associated with the linear variation of displacement through the thickness, while ψ_x and ψ_γ describe an additional higher-order contribution defined by the function F(z). Accordingly, the in-plane displacements consist of membrane, bending, and higher-order components, whereas the transverse displacement is assumed to remain constant through the thickness.

The resulting kinematic field provides a consistent representation of transverse shear deformation without the need for shear correction factors, with the shear distribution being directly governed by function F(z).

Based on these kinematic assumptions, seven degrees of freedom per node are introduced in the finite element formulation,

$$\mathrm{d} = \{u_0, v_0, w_0, \phi_x, \phi_y, \psi_x, \psi_y\}^T,$$

which enables efficient discretization within an isoparametric finite element framework.

2.2. Strain field and constitutive relations

The components of the linearized strain tensor follow from the displacement field (1) according to the small-strain theory as

$$\begin{aligned} &\varepsilon_{xx} = u_{,x},\ \varepsilon_{yy} = v_{,y},\ \gamma_{xy} = u_{,y} + v_{,x} \\ &\gamma_{xz} = u_{,z} + w_{,x},\ \gamma_{yz} = v_{,z} + w_{,y}. \end{aligned} \tag{4}$$

Substituting the displacement field (1) yields

$$\begin{aligned} &\varepsilon_{xx} = u_{0,x} + \sum_{I=1}^{2} U_x^I \Phi^I(z), \varepsilon_{yy} = v_{0,y} + \sum_{I=1}^{2} V_y^I \Phi^I(z) \\ &\gamma_{xy} = u_{0,y} + v_{0,x} + \sum_{I=1}^{2} \left(U^I_{,y} + V^I_{,x}\right)\Phi^I(z) \\ &\gamma_{xz} = w_{0,x} + \sum_{I=1}^{2} U^I \Phi^{I'}(z), \gamma_{yz} = w_{0,y} + \sum_{I=1}^{2} V^I \Phi^{I'}(z) \end{aligned} \tag{5}$$

Introducing the through-thickness shape functions and the corresponding kinematic variables from Eq. (1) yields

$$\begin{aligned} &\varepsilon_{xx} = u_{0,x} + z\phi_{x,x} + F(z)\psi_{x,x}, \varepsilon_{yy} = v_{0,y} + z\phi_{y,y} + F(z)\psi_{y,y}, \\ &\gamma_{xy} = u_{0,y} + v_{0,x} + z\left(\phi_{x,y} + \phi_{y,x}\right) + F(z)\left(\psi_{x,y} + \psi_{y,x}\right), \\ &\gamma_{xz} = w_{0,x} + \phi_x + F'(z)\psi_x, \gamma_{yz} = w_{0,y} + \phi_y + F'(z)\psi_y. \end{aligned} \tag{6}$$

For a compact representation, the in-plane strains can be expressed as

$$\boldsymbol{\varepsilon}(x,y,z) = \boldsymbol{\varepsilon}^0 + z\boldsymbol{\kappa}^{(1)} + F(z)\boldsymbol{\kappa}^{(2)}, \tag{7}$$

where

$$\boldsymbol{\varepsilon}^0 = \left\{ \begin{array}{c} u_{0,x} \\ v_{0,y} \\ u_{0,y} + v_{0,x} \end{array} \right\}, \boldsymbol{\kappa}^{(1)} = \left\{ \begin{array}{c} \phi_{x,x} \\ \phi_{y,y} \\ \phi_{x,y} + \phi_{y,x} \end{array} \right\}, \boldsymbol{\kappa}^{(2)} = \left\{ \begin{array}{c} \psi_{x,x} \\ \psi_{y,y} \\ \psi_{x,y} + \psi_{y,x} \end{array} \right\}. \tag{8}$$

The strain field is thus decomposed into membrane, bending, and higher-order contributions, while the transverse shear strains are governed by the derivative of the through-thickness shape function. The choice of the function F(z) such that $F'(\pm h/2) = 0$ ensures that the higher-order contribution to the shear strains vanishes at the free surfaces, thereby satisfying the traction-free conditions without the need for shear correction factors.

A laminated or sandwich plate composed of orthotropic layers is considered, where each k-th layer is characterized by its own elastic properties and fibre orientation $\theta^{(k)}$. Under the assumption of a plane stress state, the constitutive relations in the global coordinate system take the form

$$\boldsymbol{\sigma}^{(k)} = \overline{\boldsymbol{Q}}^{(k)}\left(\boldsymbol{\varepsilon}^{(k)} - \boldsymbol{\varepsilon}^{\text{th }(k)}\right), \tag{9}$$

where

$$\boldsymbol{\sigma}^{(k)} = \begin{Bmatrix} \sigma_{xx} \\ \sigma_{yy} \\ \tau_{xy} \\ \tau_{xz} \\ \tau_{yz} \end{Bmatrix}, \boldsymbol{\varepsilon}^{(k)} = \begin{Bmatrix} \varepsilon_{xx} \\ \varepsilon_{yy} \\ \gamma_{xy} \\ \gamma_{xz} \\ \gamma_{yz} \end{Bmatrix}, \quad \boldsymbol{\varepsilon}^{th(k)} = \begin{Bmatrix} \alpha_{xx} \\ \alpha_{yy} \\ \alpha_{xy} \\ 0 \\ 0 \end{Bmatrix}^{(k)} \Delta T. \tag{10}$$

The transformed stiffness matrix $\overline{\mathbf{Q}}^{(k)}$ depends on the fiber orientation $\theta^{(k)}$a nd can be written as

$$\overline{\boldsymbol{Q}}^{(k)} = \begin{bmatrix} \overline{Q}_{11} & \overline{Q}_{12} & \overline{Q}_{16} & 0 & 0 \\ \overline{Q}_{12} & \overline{Q}_{22} & \overline{Q}_{26} & 0 & 0 \\ \overline{Q}_{16} & \overline{Q}_{26} & \overline{Q}_{66} & 0 & 0 \\ 0 & 0 & 0 & \overline{Q}_{55} & \overline{Q}_{45} \\ 0 & 0 & 0 & \overline{Q}_{45} & \overline{Q}_{44} \end{bmatrix}^{(k)}. \tag{11}$$

The components $\overline{Q}_{ij}^{(k)}$ and the thermal expansion coefficients are obtained by standard transformation from the local to the global coordinate system.

By integrating the contributions of all layers through the thickness, in combination with the kinematics given in Eqs. (1) – (8), the corresponding membrane, bending, higher-order, and shear stiffnesses of the laminate are obtained.

2.3. Stress resultants and variational formulation

The stress resultants are defined by integration through the thickness of the laminate as

$$\boldsymbol{N} = \int_{-h/2}^{h/2} \boldsymbol{\sigma}_p dz,\ \boldsymbol{M} = \int_{-h/2}^{h/2} z\boldsymbol{\sigma}_p dz,\ \boldsymbol{P} = \int_{-h/2}^{h/2} F(z)\boldsymbol{\sigma}_p dz \tag{12}$$

where $\boldsymbol{\sigma}_p = \{\sigma_{xx}, \sigma_{yy}, \tau_{xy}\}^T$, where N, M, and P denote the membrane, bending, and higher-order resultants, respectively.

Combining the kinematic relations (7) with the constitutive relations (9) yields

$$\begin{Bmatrix} \boldsymbol{N} \\ \boldsymbol{M} \\ \boldsymbol{P} \end{Bmatrix} = \begin{bmatrix} \boldsymbol{A} & \boldsymbol{B} & \boldsymbol{A}_F \\ \boldsymbol{B} & \boldsymbol{D} & \boldsymbol{B}_F \\ \boldsymbol{A}_F & \boldsymbol{B}_F & \boldsymbol{D}_F \end{bmatrix} \begin{Bmatrix} \boldsymbol{\varepsilon}^0 \\ \boldsymbol{\kappa}^{(1)} \\ \boldsymbol{\kappa}^{(2)} \end{Bmatrix} - \begin{Bmatrix} \boldsymbol{N}^T \\ \boldsymbol{M}^T \\ \boldsymbol{P}^T \end{Bmatrix}. \tag{13}$$

The stiffness matrices are given by

$$\begin{aligned} \boldsymbol{A} &= \sum_{k=1}^{N}\int_{z_k}^{z_{k+1}} \overline{\boldsymbol{Q}}^{(k)} dz,\ \boldsymbol{B} = \sum_{k=1}^{N}\int_{z_k}^{z_{k+1}} z\overline{\boldsymbol{Q}}^{(k)} dz,\ \boldsymbol{D} = \sum_{k=1}^{N}\int_{z_k}^{z_{k+1}} z^2\overline{\boldsymbol{Q}}^{(k)} dz, \\ \boldsymbol{A}_F &= \sum_{k=1}^{N}\int_{z_k}^{z_{k+1}} F(z)\overline{\boldsymbol{Q}}^{(k)} dz,\ \boldsymbol{B}_F = \sum_{k=1}^{N}\int_{z_k}^{z_{k+1}} zF(z)\overline{\boldsymbol{Q}}^{(k)} dz,\ \boldsymbol{D}_F = \sum_{k=1}^{N}\int_{z_k}^{z_{k+1}} F^2(z)\overline{\boldsymbol{Q}}^{(k)} dz \end{aligned} \tag{14}$$

The transverse shear resultants are defined as

$$\boldsymbol{\tau} = \begin{Bmatrix} \tau_{xz} \\ \tau_{yz} \end{Bmatrix} = \boldsymbol{S}_0\gamma_0 + \boldsymbol{S}_1\gamma_1 + \boldsymbol{S}_2\gamma_2, \tag{15}$$

where the matrices S_0, S_1, and S_2 represent the effective shear stiffnesses defined through the through-thickness distribution of strains.

The governing equilibrium equations are derived using the principle of virtual work

$$\delta W_{\text{int}} - \delta W_{\text{th}} - \delta W_{\text{ext}} = 0 \tag{16}$$

The virtual work of internal forces, in accordance with the defined generalized strains and stress resultants, takes the form

$$\delta W_{int} = \int_\Omega \left(\delta\boldsymbol{\varepsilon}^{0T}\boldsymbol{N} + \delta\boldsymbol{\kappa}^{(1)T}\boldsymbol{M} + \delta\boldsymbol{\kappa}^{(2)T}\boldsymbol{P} + \delta\boldsymbol{\gamma}^T\boldsymbol{Q}\right)d\Omega \tag{17}$$

where N, M, P, and Q are the vectors of membrane, bending, higher-order, and shear resultants, respectively.

The thermal contribution is introduced through the corresponding resultants

$$\begin{Bmatrix} \boldsymbol{N} \\ \boldsymbol{M} \\ \boldsymbol{P} \end{Bmatrix} = \begin{bmatrix} \boldsymbol{A} & \boldsymbol{B} & \boldsymbol{A}_F \\ \boldsymbol{B} & \boldsymbol{D} & \boldsymbol{B}_F \\ \boldsymbol{A}_F & \boldsymbol{B}_F & \boldsymbol{D}_F \end{bmatrix} \begin{Bmatrix} \boldsymbol{\varepsilon}^0 \\ \boldsymbol{\kappa}^{(1)} \\ \boldsymbol{\kappa}^{(2)} \end{Bmatrix} - \begin{Bmatrix} \boldsymbol{N}^T \\ \boldsymbol{M}^T \\ \boldsymbol{P}^T \end{Bmatrix}, \tag{18}$$

which leads to

$$\delta W_{th} = \int_\Omega \left(\delta\boldsymbol{\varepsilon}^{0T}\boldsymbol{N}^T + \delta\boldsymbol{\kappa}^{(1)T}\boldsymbol{M}^T + \delta\boldsymbol{\kappa}^{(2)T}\boldsymbol{P}^T\right)d\Omega \tag{19}$$

The virtual work of external loads is given by

$$\delta W_{ext} = \int_\Omega q\delta w_0 d\Omega + \int_\Gamma \boldsymbol{t}^T\delta\boldsymbol{u}d\Gamma \tag{20}$$

Finally, the governing equation is obtained as

$$\begin{aligned} &\int_\Omega \left(\delta\boldsymbol{\varepsilon}^{0T}\boldsymbol{N} + \delta\boldsymbol{\kappa}^{(1)T}\boldsymbol{M} + \delta\boldsymbol{\kappa}^{(2)T}\boldsymbol{P} + \delta\boldsymbol{\gamma}^T\boldsymbol{Q}\right)d\Omega \\ -&\int_\Omega \left(\delta\boldsymbol{\varepsilon}^{0T}\boldsymbol{N}^T + \delta\boldsymbol{\kappa}^{(1)T}\boldsymbol{M}^T + \delta\boldsymbol{\kappa}^{(2)T}\boldsymbol{P}^T\right)d\Omega - \delta W_{\text{ext}} = 0 \end{aligned} \tag{21}$$

The temperature field is assumed to vary both in the plane of the plate and through the thickness, and is expressed as

$$T(x,y,z) = T_1(x,y) + \frac{z}{h}T_2(x,y) + \frac{F(z)}{h}T_3(x,y), \tag{22}$$

where the functions T_1, T_2, and T_3 describe the corresponding components of the temperature distribution, while F(z) denotes the through-thickness shape function introduced in the kinematic model.

The thermal strains in each layer take the form

$$\boldsymbol{\varepsilon}^{\text{th}} = \boldsymbol{\alpha}T(x,y,z), \tag{23}$$

where $\alpha = \{\alpha_{xx}, \alpha_{\gamma\gamma}, \alpha_{x\gamma}\}^T$ is the vector of thermal expansion coefficients in the global coordinate system and depends on the layer orientation.

By integrating through the thickness, in accordance with the kinematics and constitutive relations, the thermally induced resultants N^T, M^T, and P^T are obtained, corresponding to the membrane, bending, and higher-order contributions, and directly enter the variational formulation of the problem.

2.4. Through-thickness shape function

The distribution of transverse shear deformation is governed by the shape function F(z), whose first derivative directly enters the expressions for shear strains. Consequently, the choice of F(z) directly determines the through-thickness shear distribution, as well as the regularity of the strain field and the numerical properties of the formulation.

To construct a function consistent with the adopted kinematics, a dimensionless coordinate is introduced

$$\zeta = \frac{z}{h}, \zeta \in [-1/2, 1/2], \tag{24}$$

which leads to the representation

$$F(z) = h\Phi(\zeta),\ \frac{dF}{dz} = \Phi'(\zeta), \tag{25}$$

thereby reducing the problem to the determination of the function Φ′(ζ), which directly governs the distribution of shear strains through the thickness.

The function Φ′(ζ) is constructed to satisfy the following conditions:

$$\Phi'(\pm 1/2) = 0,\ \Phi'(-\zeta) = \Phi'(\zeta),\ \Phi'(0) = 1, \tag{26}$$

with the requirement that $\Phi \in C^{\infty}[-1/2, 1/2]$. These conditions ensure the vanishing of the higher-order shear contribution at the free surfaces, a symmetric distribution of strains, and a unique normalization of the function.

In accordance with these requirements, an exponentially modulated function is introduced

$$\Phi'(\zeta) = \left(1 - 4\zeta^2\right)e^{-a\zeta^2}, a > 0, \tag{27}$$

where the polynomial term enforces zero values at the surfaces, while the exponential term enables continuous control over the distribution of transverse shear deformation.

Integration yields

$$\Phi(\zeta) = \int_0^{\zeta} \left(1 - 4s^2\right)e^{-as^2} ds \tag{28}$$

leading to the closed-form expression

$$\Phi(\zeta) = \frac{\sqrt{\pi}(a-2)}{2a^{3/2}} erf\left(\sqrt{a}\zeta\right) + \frac{2\zeta}{a}e^{-a\zeta^2} \tag{29}$$

The second derivative of the function takes the explicit form

$$\Phi''(\zeta) = -2\zeta e^{-a\zeta^2}\left[4 + a\left(1 - 4\zeta^2\right)\right], \tag{30}$$

which allows for a direct assessment of the curvature of the distribution.

The parameter a governs the shape of the function and introduces an additional degree of freedom into the model. Its optimal value is determined variationally by minimizing the functional

$$J(a) = \int_{-1/2}^{1/2} (\Phi''(\zeta; a))^2 d\zeta, a^* = \underset{a>0}{\operatorname{argmin}} J(a) \tag{31}$$

thereby minimizing a measure of the curvature of the shear deformation distribution and favouring smooth functions with desirable numerical properties.

The minimization of the functional defined in Eq. (31) is performed with respect to the single scalar parameter a. Since the functional is formulated in terms of the dimensionless thickness coordinate ζ and depends exclusively on the adopted analytical form of Φ′(ζ; a), it is independent of the laminate stacking sequence, material properties, thickness ratio, and loading condition. A one-dimensional numerical minimization yields a unique minimum within the admissible domain a > 0 at a* = 4.036. This value is used throughout all numerical examples presented in this study.

It should be noted that the functional defined in Eq. (31) does not represent the complete physical transverse shear strain energy of the laminate. Rather, it constitutes an auxiliary variational functional used to determine the governing parameter of the thickness shape function. Since the transverse shear strains are directly governed by F′(z), the minimization of this functional influences the resulting through-thickness shear deformation distribution and, consequently, the associated shear effects.

The analysis of limiting cases shows that, for a → 0,

$$\Phi'(\zeta) \approx \left(1 - 4\zeta^2\right)\left(1 - a\zeta^2\right), \tag{32}$$

while for a → ∞,

$$\Phi'(\zeta) \sim e^{-a\zeta^2} \tag{33}$$

which leads to the localization of shear deformation in the vicinity of the mid-surface. In this way, the parameter a enables a continuous transition between global and localized shear distributions.

Since the shear strains are proportional to F′(z), or equivalently Φ′(ζ), the choice of the shape function directly determines the distribution of transverse shear energy through the thickness. This establishes a direct link between the mathematical construction of the shape function and the physical response of the plate.

The transverse shear energy can be expressed as

$$U_s = \frac{1}{2}\int_{-h/2}^{h/2} G(z)\gamma_{xz}^2 dz + \frac{1}{2}\int_{-h/2}^{h/2} G(z)\gamma_{yz}^2 dz \tag{34}$$

Accordingly, the construction of Φ′(ζ) may be interpreted as controlling the through-thickness distribution of transverse shear deformation and, consequently, influencing the associated shear energy distribution. Smooth functions with controlled curvature generally lead to more regular deformation fields and improved numerical behaviour of the discretized system.

3. Finite element formulation

3.1. Displacement field approximation

For the discretization of the plate, a four-node isoparametric quadrilateral finite element is employed [46]. In accordance with the adopted seven-degree-of-freedom kinematic model, a vector of nodal variables is defined at each node

$$\boldsymbol{d}_i^e = \left\{ u_i^e\, v_i^e\, w_i^e\, \phi_{xi}^e\, \phi_{yi}^e\, \psi_{xi}^e\, \psi_{yi}^e \right\}^T, i = 1, \ldots, 4, \tag{35}$$

where u_i^e, v_i^e, w_i^e denote the mid−surface translations, while ϕ_x, ϕ_y i ψ_x, ψ_y represent the corresponding generalized kinematic variables.

The displacement field within the element Ω^e is approximated using bilinear shape functions $N_i(\xi, \eta)$, such that

$$\boldsymbol{u}(x, y) = \sum_{i=1}^{4} N_i(x, y)\boldsymbol{d}_i^e, \tag{36}$$

Relation (36) can be written in a compact form as

$$\boldsymbol{u}(x, y) = \boldsymbol{N}(x, y)\boldsymbol{d}^e, \tag{37}$$

where

$$\boldsymbol{d}^e = \begin{Bmatrix} \boldsymbol{d}_1^e \\ \boldsymbol{d}_2^e \\ \boldsymbol{d}_3^e \\ \boldsymbol{d}_4^e \end{Bmatrix}, \boldsymbol{N} = [N_1\boldsymbol{I}_7\, N_2\boldsymbol{I}_7\, N_3\boldsymbol{I}_7\, N_4\boldsymbol{I}_7]. \tag{38}$$

In this way, a direct C^0 discretization of the adopted model is achieved.

3.2. Strain–displacement relations

The generalized strains are expressed as linear functions of the element nodal variables

$$\boldsymbol{\varepsilon}^0 = \boldsymbol{B}_m \boldsymbol{d}^e, \boldsymbol{\kappa}^{(1)} = \boldsymbol{B}_\phi \boldsymbol{d}^e, \boldsymbol{\kappa}^{(2)} = \boldsymbol{B}_\psi \boldsymbol{d}^e \tag{39}$$

where the matrices $\mathbf{B}_m$, $\mathbf{B}_\phi$ i $\mathbf{B}_\psi$ are derived from the gradients of the interpolation functions following the standard finite element procedure described in [46]. For a four-node quadrilateral element, the corresponding matrices take the form

$$\boldsymbol{B}_m = \begin{bmatrix} N_{1,x} & 0 & 0 & 0 & 0 & 0 & 0 & \cdots & N_{4,x} & 0 & 0 & 0 & 0 & 0 & 0 \\ 0 & N_{1,y} & 0 & 0 & 0 & 0 & 0 & \cdots & 0 & N_{4,y} & 0 & 0 & 0 & 0 & 0 \\ N_{1,y} & N_{1,x} & 0 & 0 & 0 & 0 & 0 & \cdots & N_{4,y} & N_{4,x} & 0 & 0 & 0 & 0 & 0 \end{bmatrix},$$
$$\boldsymbol{B}_\phi = \begin{bmatrix} 0 & 0 & 0 & N_{1,x} & 0 & 0 & 0 & \cdots & 0 & 0 & 0 & N_{4,x} & 0 & 0 & 0 \\ 0 & 0 & 0 & 0 & N_{1,y} & 0 & 0 & \cdots & 0 & 0 & 0 & 0 & N_{4,y} & 0 & 0 \\ 0 & 0 & 0 & N_{1,y} & N_{1,x} & 0 & 0 & \cdots & 0 & 0 & 0 & N_{4,y} & N_{4,x} & 0 & 0 \end{bmatrix},$$
$$\boldsymbol{B}_\psi = \begin{bmatrix} 0 & 0 & 0 & 0 & 0 & N_{1,x} & 0 & \cdots & 0 & 0 & 0 & 0 & 0 & N_{4,x} & 0 \\ 0 & 0 & 0 & 0 & 0 & 0 & N_{1,y} & \cdots & 0 & 0 & 0 & 0 & 0 & 0 & N_{4,y} \\ 0 & 0 & 0 & 0 & 0 & N_{1,y} & N_{1,x} & \cdots & 0 & 0 & 0 & 0 & 0 & N_{4,y} & N_{4,x} \end{bmatrix}. \tag{40}$$

The transverse shear strains, in accordance with relation (6), are obtained as

$$\gamma = (\boldsymbol{B}_{s0} + F'(z)\boldsymbol{B}_{s1})\boldsymbol{d}^e, \tag{41}$$

where the matrices $\mathbf{B}_{s0}$ i $\mathbf{B}_{s1}$ represent the basic and higher-order contributions to the shear kinematics.

3.3. Element equations

The finite element equations are derived using the principle of minimum total potential energy [41]

$$\Pi^e = U^e - W^e \tag{42}$$

where U^e denotes the strain energy and W^e the work of external loads.

The generalized strains are expressed as

$$\boldsymbol{E} = \begin{Bmatrix} \boldsymbol{\varepsilon}^0 \\ \boldsymbol{\kappa}^{(1)} \\ \boldsymbol{\kappa}^{(2)} \end{Bmatrix} = \boldsymbol{B}_g \boldsymbol{d}^e, \boldsymbol{B}_g = \begin{bmatrix} \boldsymbol{B}_m \\ \boldsymbol{B}_\phi \\ \boldsymbol{B}_\psi \end{bmatrix}. \tag{43}$$

while the generalized force resultants are related to the strains through the laminate constitutive relations

$$\boldsymbol{R} = \begin{Bmatrix} \boldsymbol{N} \\ \boldsymbol{M} \\ \boldsymbol{P} \end{Bmatrix} = \boldsymbol{D}_L \boldsymbol{E} - \boldsymbol{R}^T, \tag{44}$$

where the laminate stiffness matrix is defined as

$$\boldsymbol{D}_L = \begin{bmatrix} \boldsymbol{A} & \boldsymbol{B} & \boldsymbol{A}_F \\ \boldsymbol{B} & \boldsymbol{D} & \boldsymbol{B}_F \\ \boldsymbol{A}_F & \boldsymbol{B}_F & \boldsymbol{D}_F \end{bmatrix}. \tag{45}$$

The transverse shear strains are obtained as

$$\boldsymbol{\gamma} = \boldsymbol{B}_s(z)\boldsymbol{d}^e, \boldsymbol{B}_s(z) = \boldsymbol{B}_{s0} + F'(z)\boldsymbol{B}_{s1}, \tag{46}$$

and the corresponding shear resultants as

$$\boldsymbol{Q} = \boldsymbol{S}(z)\gamma, \boldsymbol{S}(z) = \boldsymbol{S}_0 + F'(z)\boldsymbol{S}_1 + F'^2(z)\boldsymbol{S}_2 \tag{47}$$

The element strain energy is given by

$$U^e = \frac{1}{2}\int_{\Omega^e} \boldsymbol{E}^T \boldsymbol{D}_L \boldsymbol{E} d\Omega + \frac{1}{2}\int_{\Omega^e} \gamma^T \boldsymbol{S} \gamma d\Omega \tag{48}$$

Application of the stationarity condition $\delta\Pi^e = 0$ yields the finite element equation

$$\boldsymbol{K}^e \boldsymbol{d}^e = \boldsymbol{f}^e \tag{49}$$

where the element stiffness matrix is defined as

$$\boldsymbol{K}^e = \int_{\Omega^e} \boldsymbol{B}_g^T \boldsymbol{D}_L \boldsymbol{B}_g d\Omega + \int_{\Omega^e} \boldsymbol{B}_s^T \boldsymbol{S} \boldsymbol{B}_s d\Omega \tag{50}$$

while thermal effects are introduced through the equivalent load vector

$$\boldsymbol{f}_{th}^e = \int_{\Omega^e} \left(\boldsymbol{B}_m^T \boldsymbol{N}^T + \boldsymbol{B}_\phi^T \boldsymbol{M}^T + \boldsymbol{B}_\psi^T \boldsymbol{P}^T \right) d\Omega \tag{51}$$

3.4. Numerical implementation

The element stiffness matrices and corresponding load vectors are evaluated by numerical integration over the element domain and through the laminate thickness. In-plane integration is performed using Gauss–Legendre quadrature in the isoparametric coordinate system [46], while through-thickness integration is carried out layer by layer, thereby explicitly accounting for the discrete variation of material properties and fibre orientations.

The membrane, bending, and higher-order contributions are constructed from the matrices $\mathbf{B}_m$, $\mathbf{B}_\phi$ i $\mathbf{B}_\psi$, together with the corresponding laminate stiffness matrices $\mathbf{A}$, $\mathbf{B}$, $\mathbf{D}$, $\mathbf{A}_F$, $\mathbf{B}_F$ i $\mathbf{D}_F$. Within this framework, the influence of the proposed shape function F(z) is consistently incorporated into the effective stiffnesses through terms involving $F(z)$, $zF(z)$, $F^2(z)$, $F'(z)$ i $F'^2(z)$.

Special attention is required for transverse shear due to the well-known shear locking phenomenon in low-order elements. To alleviate this issue, the MITC4 interpolation is adopted [47], in which the shear strains are evaluated from tying values defined at characteristic points of the element rather than directly from the gradients of the interpolated field. This approach ensures a stable approximation of shear deformation without loss of accuracy, while remaining fully compatible with the higher-order kinematics

$$\gamma_{xz} = \boldsymbol{B}_{sx}\boldsymbol{d}^e, \gamma_{yz} = \boldsymbol{B}_{sy}\boldsymbol{d}^e \tag{52}$$

with the corresponding structures

$$\boldsymbol{B}_{sx} = \boldsymbol{B}_{sx}^0 + F'(z)\boldsymbol{B}_{sx}^1, \boldsymbol{B}_{sy} = \boldsymbol{B}_{sy}^0 + F'(z)\boldsymbol{B}_{sy}^1, \tag{53}$$

Thermal effects are introduced at the layer level through the prescribed temperature field and the associated thermal strains, after which the thermally induced resultants $\mathbf{N}^T$, $\mathbf{M}^T$ i $\mathbf{P}^T$ are obtained by integration through the thickness. Their contribution at the element level is computed by projection onto the interpolation space in the form

$$\boldsymbol{f}_{th}^e = \int_{\Omega^e} \left(\boldsymbol{B}_m^T \boldsymbol{N}^T + \boldsymbol{B}_\phi^T \boldsymbol{M}^T + \boldsymbol{B}_\psi^T \boldsymbol{P}^T \right) d\Omega \tag{54}$$

which represents a consistent thermal load vector within the variational formulation.

Following the evaluation of element matrices and vectors, the global system of equations is assembled using the standard connectivity-based procedure

$$\boldsymbol{K}\boldsymbol{d} = \boldsymbol{f}_m + \boldsymbol{f}_{th}, \tag{55}$$

where $\mathbf{f}_m$ i $\mathbf{f}_{\mathrm{th}}$ denote the global mechanical and thermal load vectors.

The proposed implementation enables a consistent incorporation of the layered structure, higher-order kinematics, and thermal effects, while maintaining stable numerical behavior without the occurrence of shear locking.

4. Numerical results and discussion

To assess the accuracy and numerical robustness of the proposed formulation, a well-established reference problem of thermo-mechanical bending of an orthotropic plate with simply supported edges (SSSS) is considered, enabling direct comparison with high-accuracy reference solutions. The plate material is modelled as an orthotropic composite with properties defined as

$$E_1 = 25E_2, G_{12} = 0.5E_2, G_{13} = 0.5E_2, G_{23} = 0.2E_2, \nu_{12} = 0.25,$$

while two values of the thermal expansion ratio are considered, $\alpha_2/\alpha_1 = 3$ and $\alpha_2/\alpha_1 = 1125$. The temperature field is prescribed in two prescribed forms

$$\begin{aligned} SSL: a)\ Type\, I\ T(x,y,z) &= \frac{z}{h}\Delta T\sin\left(\frac{\pi x}{a}\right)\sin\left(\frac{\pi y}{b}\right), \\ b)\ Type\, II\ T(x,y,z) &= \frac{2z}{h}\Delta T\sin\left(\frac{\pi x}{a}\right)\sin\left(\frac{\pi y}{b}\right), \\ UDL: T(x,y,z) &= \frac{z}{h}\Delta T, \end{aligned} \tag{56}$$

while the mechanical load is defined as

$$q(x,y) = q_0\sin\left(\frac{\pi x}{a}\right)\sin\left(\frac{\pi y}{b}\right). \tag{57}$$

The numerical analysis is performed using a four-node quadrilateral finite element with seven degrees of freedom per node. In-plane integration is carried out using Gauss–Legendre quadrature, while through-thickness integration is performed layer-wise. Transverse shear strains are interpolated using the MITC4 technique, thereby eliminating shear locking typically associated with low-order formulations.

4.1. Validation against reference solutions

For the verification of the proposed model, an orthotropic rectangular plate of dimensions a × b is considered, with aspect ratios a/b = 1 and a/h = 10, corresponding to a moderately thick plate in which transverse shear and interlaminar effects are significant, yet remain within the validity range of equivalent single-layer (ESL) theories.

Under thermal loading, the central deflection is expressed in the dimensionless form

$$\widehat{w} = \frac{10h}{\alpha_1 \Delta T b^2} w \tag{58}$$

where w denotes the central deflection of the plate, and $\alpha_1\Delta T$ represents the reference thermal parameter. This normalization removes the influence of absolute magnitudes and enables direct comparison with results reported in the literature.

The convergence of the finite element solution is assessed through successive mesh refinement, with the dimensionless central deflection ŵ used as the primary measure of accuracy and numerical stability.

The results presented in Table 1 exhibit a monotonic and stable convergence behaviour without oscillations under mesh refinement. As shown in Table 2, the rapid stabilization of the central deflection indicates that the proposed element accurately captures the dominant deformation mechanisms even on relatively coarse meshes.

The relative error drops below 0.005% already for a 40 × 40 mesh, confirming the high approximation capability of the formulation and its efficiency for practical analyses without the need for excessively fine discretization.

The monotonic convergence observed in Table 1, together with the rapid stabilization of the normalized central deflection under mesh refinement, indicates that the numerical response is effectively mesh-independent for the adopted discretization. Since analytical or high-fidelity reference solutions are available for all benchmark problems considered in this study, the numerical accuracy is assessed directly through relative deviations with respect to these reference solutions.

For further validation, the converged solution is compared with reference results available in the literature for identical geometric and material conditions.

The obtained result ŵ = 1.0438 shows excellent agreement with the reference solution of Cetković [37], with a relative deviation of approximately 0.17%. At the same time, the nearly identical agreement with the FSDT result (difference below 0.02%) further confirms the high accuracy of the global response, while the discrepancy with respect to the CLPT solution is expected due to the neglect of transverse shear deformation in the classical plate theory.

The achieved accuracy is directly related to the improved modelling of transverse shear deformation, which in the proposed formulation enables an energetically consistent distribution of deformation energy through the plate thickness. In contrast to standard ESL approaches, where the shear deformation distribution is prescribed a priori, it is here determined as part of the solution, thereby eliminating the need for shear correction factors and yielding a more realistic prediction of the effective bending stiffness and deflection.

Combined with the stable convergence behaviour, these results

Table 1
Mesh convergence of the normalized central deflection ŵ for an orthotropic rectangular plate under sinusoidal thermal loading (Type I) (a/b = 1, a/h = 10).

Mesh	Number of elements	$\widehat{w}$	Relative error (%)
10 × 10	100	1.0445	0.0635
20 × 20	400	1.0440	0.0165
40 × 40	1600	1.0438	0.0040
80 × 80	6400	1.0438	0.0008
160 × 160	25,600	1.0438	0.0000

Table 2
Comparison of the normalized central deflection ŵ with reference solutions for an orthotropic rectangular plate under sinusoidal thermal loading (Type I) (a/b = 1, a/h = 10).

Method	$\widehat{w}$
CLPT [37]	1.0312
FSDT [37]	1.0440
Četković [37]	1.0420
Present model (this work)	1.0438

Table 3
Comparison of the normalized central deflection ŵ with reference solutions for different a/b and b/h ratios under uniform thermal loading.

(b/h)	Model	(a/b = 1)	(a/b = 1.5)	(a/b = 2)	(a/b = 2.5)	(a/b = 3)
10	LW [37]	1.4568	3.1309	4.5304	5.2906	5.5513
	FSDT [9]	1.4603	3.1321	4.5966	5.4269	5.6987
	CLPT [9]	1.4331	3.1344	4.6346	5.4736	5.7330
	Present model	1.4604	3.1331	4.5980	5.4284	5.7000
	Error (%)	0.248	0.069	1.493	2.604	2.678
20	LW [37]	1.4401	3.1340	4.6033	5.4155	5.6736
	FSDT [9]	1.4409	3.1339	4.6243	5.4609	5.7239
	CLPT [9]	1.4331	3.1344	4.6346	5.4736	5.7330
	Present model	1.4413	3.1348	4.6254	5.4620	5.7250
	Error (%)	0.084	0.024	0.481	0.859	0.906
100	LW [37]	1.4338	3.1350	4.6341	5.4719	5.7317
	FSDT [9]	1.4334	3.1343	4.6342	5.4729	5.7327
	CLPT [9]	1.4331	3.1344	4.6346	5.4734	5.7330
	Present model	1.4339	3.1352	4.6352	5.4739	5.7337
	Error (%)	0.010	0.008	0.024	0.037	0.034

Table 4
Comparison of the normalized central deflection $\hat{w}$ for a cross-ply [0/90/90/0] laminated plate under uniform thermal loading.

b/h	Model	$a/b=1$	$a/b=1.5$	$a/b=2$	$a/b=2.5$	$a/b=3$
10	LW [37]	1.6013	2.5688	2.8333	2.8011	2.7083
	FSDT [9]	1.5452	2.5733	2.8961	2.8045	2.5921
	CLPT [9]	1.5316	2.6350	2.9507	2.8245	2.5859
	Present model	1.5515	2.5537	2.8729	2.7926	2.5923
	Error (%)	3.112	0.587	1.397	0.303	4.282
20	LW [37]	1.5912	2.6739	2.9733	2.8771	2.6918
	FSDT [9]	1.5357	2.6169	2.9352	1.8191	2.5877
	LW [34]	1.5316	2.6350	2.9507	1.8245	2.5859
	Present model	1.5382	2.6103	2.9278	2.8156	2.5881
	Error (%)	3.333	2.377	1.530	2.137	3.853
100	LW [37]	1.5860	2.7291	3.0618	2.9400	2.7014
	FSDT [9]	1.5318	2.6343	2.9500	2.8243	2.5859
	CLPT [9]	1.5316	2.6350	2.9507	2.8245	2.5859
	Present model	1.5323	2.6345	2.9502	2.8246	2.5867
	Error (%)	3.385	3.466	3.646	3.924	4.247

Table 5
Comparison of the normalized central deflection $\hat{w}$ for a cross-ply [0/90/90/0] laminated plate under sinusoidal thermal loading (Type I).

(b/h)	Model	(a/b = 1)	(a/b = 1.5)	(a/b = 2)	(a/b = 2.5)	(a/b = 3)
10	LW [37]	1.0778	1.7218	1.9540	2.0088	2.0179
	FSDT [9]	1.0421	1.7130	1.9680	1.9807	1.9227
	CLPT [9]	1.0312	1.7442	1.9925	1.9872	1.9181
	Present model	1.0645	1.7376	1.9917	2.0041	1.9454
	Error (%)	1.234	0.917	1.931	0.235	3.594
20	LW [37]	1.0708	1.7771	2.0247	2.0407	1.9999
	FSDT [9]	1.0343	1.7339	1.9858	1.9854	1.9193
	CLPT [9]	1.0312	1.7422	1.9925	1.9872	1.9181
	Present model	1.0450	1.7497	2.0005	1.9975	1.9292
	Error (%)	2.414	1.542	1.197	2.116	3.537
100	LW [37]	1.0680	1.8050	2.0680	2.0677	2.0008
	FSDT [9]	1.0313	1.7419	1.9923	1.9871	1.9181
	CLPT [9]	1.0312	1.7422	1.9925	1.9872	1.9181
	Present model	1.0328	1.7448	1.9949	1.9890	1.9194
	Error (%)	3.292	3.334	3.533	3.808	4.070

demonstrate that the proposed finite element provides a reliable and physically consistent approximation of the thermo-mechanical response of orthotropic composite plates over a wide range of geometric configurations.

The results presented in Table 3 confirm consistently high accuracy of the formulation over the entire range of geometric parameters considered. For thin plates (b/h = 100), the relative error remains below 0.04%, while for moderately thin plates (b/h = 20) it does not exceed 1%. For moderately thick plates (b/h = 10), the maximum deviation is approximately 2.7%, with the largest differences observed at higher a/b ratios, where bending–shear coupling becomes more pronounced.

In Tables 3–5, the relative error is calculated with respect to the layerwise solution reported by Četković [37], which is used as the high-fidelity reference solution.

The results presented in Table 3 confirm consistently high accuracy of the formulation over the entire range of geometric parameters considered. For thin plates (b/h = 100), the relative error remains below 0.04%, while for moderately thin plates (b/h = 20) it does not exceed 1%. For moderately thick plates (b/h = 10), the maximum deviation is approximately 2.7%, with the largest differences observed at higher a/b ratios, where bending–shear coupling becomes more pronounced.

The formulation consistently captures the transition of the dominant deformation mechanism with changing geometry: as b/h increases, shear effects diminish, whereas for lower b/h ratios they remain properly represented without loss of accuracy. This behavior can be directly attributed to the adopted through-thickness shape function, which enables a consistent representation of transverse shear effects across different regimes.

Overall, the results demonstrate that the proposed model provides a reliable and physically consistent approximation of the structural response over a wide range of thickness-to-span ratios, while retaining the computational efficiency of ESL-type approaches.

4.2. Laminated plates under thermal loading

Following the verification on the orthotropic plate, a more demanding case is considered for a laminated composite plate with a symmetric cross-ply configuration [0/90/90/0], which involves through-thickness heterogeneity, material discontinuities, and pronounced interlaminar interactions that significantly influence the distribution of stresses and deformations.

The plate is subjected to uniform thermal loading (UDL), and the central deflection is evaluated over a wide range of geometric parameters, including different aspect ratios a/b and thickness ratios b/h.

The results presented in Table 4 show stable and consistent behavior of the formulation across all considered configurations. The obtained values are in good agreement with the reference solutions available in the literature, with discrepancies remaining within a few percent throughout the analyzed parameter range.

Compared to the orthotropic case, slightly larger deviations are observed, which is expected due to the increased complexity of laminated structures. While layer wise approaches explicitly capture interlaminar discontinuities in stress and strain fields, equivalent single-layer (ESL) theories rely on a homogenized representation through the thickness, which inevitably leads to some loss of local accuracy in the presence of pronounced interlaminar effects.

Nevertheless, the proposed ESL–HSDT formulation accurately reproduces the global thermo-mechanical response of the laminate, while maintaining a significantly lower computational cost compared to layer wise models. The achieved accuracy can be attributed to the manner in which the through-thickness distribution is represented in the model, with the adopted shape function F(z) enabling a consistent incorporation of transverse shear effects across different deformation regimes without the need for additional correction factors.

Furthermore, as the b/h ratio increases, a gradual reduction in discrepancies with respect to the reference solutions is observed, which is consistent with theoretical expectations, since the influence of transverse shear deformation diminishes for thinner plates. Such asymptotic behavior further confirms the consistency of the formulation across different thickness regimes.

These results indicate that, despite the inherent limitations of ESL approaches, the proposed formulation can be reliably applied to the analysis of laminated plates over a wide range of geometric parameters, while preserving the accuracy of the global response.

As an extension of the previous analysis, the case of sinusoidal thermal loading (SSL) is considered, introducing spatial variation of the temperature field in the plate plane. This type of loading leads to a stronger coupling between bending and transverse shear, thereby providing a more demanding assessment of the formulation's ability to consistently represent through-thickness kinematics.

The analysis is carried out for a laminated plate with a [0/90/90/0] configuration, with the central deflection evaluated for different a/b and b/h ratios.

The results presented in Table 5 demonstrate consistent behavior of the formulation across the entire range of geometric parameters considered, with good agreement with the reference solutions available in the literature.

Compared to the case of uniform thermal loading, slightly larger deviations are observed, which is expected due to the more complex deformation state and the stronger coupling between bending and transverse shear induced by the spatially varying temperature field. Nevertheless, the discrepancies remain limited and do not exhibit a systematic trend, indicating the robustness of the formulation under different loading conditions.

The formulation consistently captures the variation of the central deflection with changing geometric parameters. As the b/h ratio increases, the differences with respect to the reference solutions decrease, in agreement with theoretical expectations, since the influence of transverse shear deformation diminishes for thinner plates.

The achieved accuracy can be attributed to the manner in which the through-thickness distribution is represented in the model, with the adopted shape function F(z) enabling a stable and consistent representation of transverse shear effects even under spatially varying loading conditions, thereby capturing the dominant mechanisms governing the global response of the laminate.

To gain deeper insight into the mechanisms governing the thermo-mechanical response of the laminated plate, the through-thickness stress distribution is examined for the case of sinusoidal thermal loading (Type II).

Unlike mechanical loading, where the stress state is directly induced by external forces, in the thermal case stresses arise from the mismatch of free thermal strains between layers with different coefficients of thermal expansion. As a result, the through-thickness stress distribution becomes strongly dependent on the adopted kinematic description and the model's ability to consistently represent interlaminar interactions.

The following diagrams present the distributions of normal and shear stresses across the laminate thickness, providing direct insight into the stress state and its sensitivity to the assumed through-thickness kinematics.

Fig. 1 presents the through-thickness distribution of the normalized transverse shear stress $\bar{\tau}_{xz}$ in a [0/90/90/0] laminate under sinusoidal thermal loading for different a/h ratios. The distribution is smooth and nonlinear, with the shear stress naturally satisfying the traction-free condition $\bar{\tau}_{xz} = 0$ at the outer surfaces ($z/h = \pm 0.5$).

A characteristic feature is that the extrema are not located at the mid-plane ($z/h = 0$), but rather in the vicinity of $z/h \approx \pm 0.25$, close to the ply interfaces, while a local minimum is observed at the laminate mid-surface. This behavior directly reflects the layered architecture and the mismatch of thermal strains between plies of different orientations, leading to a redistribution of shear stresses away from the mid-plane.

The a/h ratio primarily affects the intensity of the distribution: as a/h increases, the amplitude of the shear stress decreases and the through-thickness gradients become less pronounced, while the location of the extrema remains nearly unchanged. This indicates that the shape of the distribution is governed predominantly by interlaminar interactions, whereas geometric parameters mainly influence their magnitude.

The distribution is symmetric with respect to the mid-plane, consistent with the symmetric stacking sequence, yet it clearly demonstrates that the maximum shear stresses are controlled by local through-thickness effects rather than by the global kinematics of the plate.

Fig. 2 shows a comparison of the $\bar{\tau}_{xz}$ distribution obtained using different through-thickness shape functions under sinusoidal thermal loading ($a/h = 4$, $a/b = 1$). The present results exhibit an almost complete agreement with reference solutions, with minor differences confined to narrow regions near the extrema and transition zones.

The observed discrepancies can be attributed to differences in the approximation of the through-thickness displacement field, without affecting the overall shape of the distribution or the location of its characteristic features. This indicates that the choice of shape function primarily influences the local numerical accuracy, while the underlying mechanism governing the transverse shear stress distribution remains unchanged.

The agreement achieved confirms that the proposed shape function F(z) provides a consistent representation of through-thickness shear effects under spatially varying thermal loading, while preserving the essential physical characteristics of stress distribution in laminated composites.

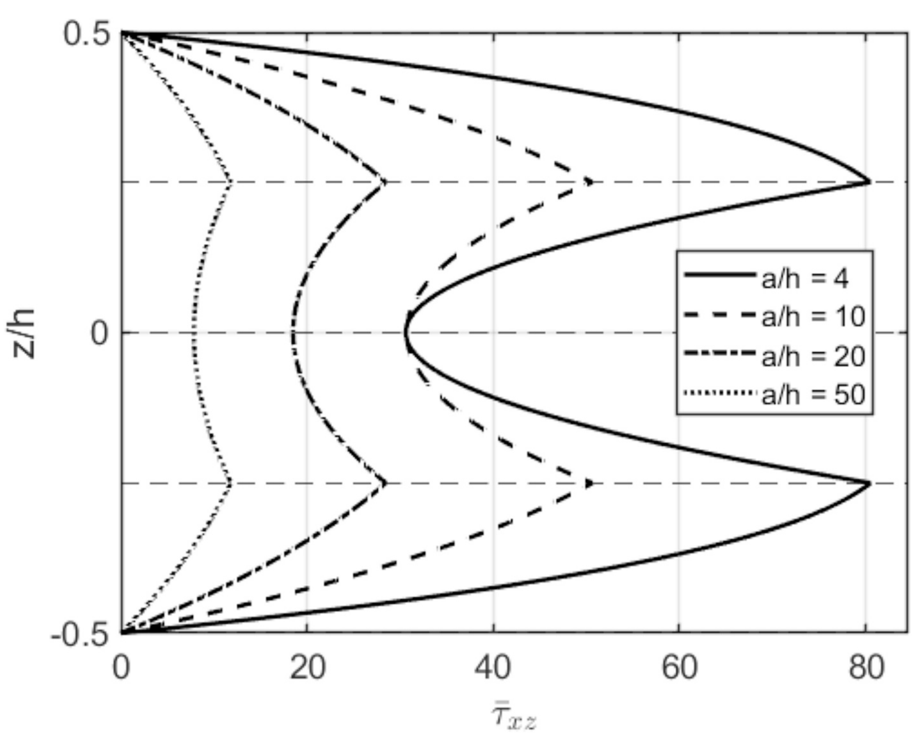

Fig. 1. Through-thickness distribution of the normalized transverse shear stress $\bar{\tau}_{xz}$ in a [0/90/90/0] laminate for different a/h ratios under sinusoidal thermal loading (Type II) ($a/b = 1$).

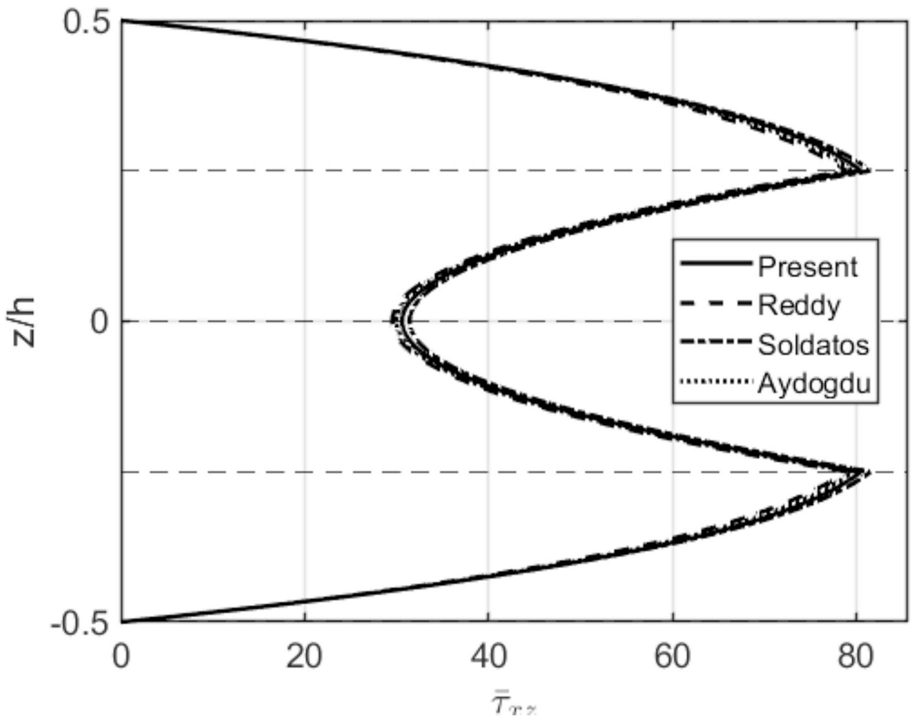

Fig. 2. Influence of the through-thickness shape function on the distribution of the normalized transverse shear stress τ¯xz in a [0/90/90/0] laminate under sinusoidal thermal loading (Type II) (a/h = 4, a/b = 1).

4.3. Laminated plate under mechanical loading

In this section, the bending and shear response of a laminated composite plate with a symmetric cross-ply configuration [0/90/90/0] subjected to mechanical loading is investigated. The analysis focuses on the central deflection and the through-thickness stress distribution as functions of the plate geometric parameters.

The plate is subjected to a sinusoidally distributed transverse load defined in Eq. (57), representing a standard benchmark case for simply supported plates and enabling direct comparison with reference solutions available in the literature.

The results are presented in dimensionless form, with normalization defined in terms of the reference load q_0, the elastic modulus E_2, and the characteristic geometric parameters of the plate. The normalized deflection and stresses are given by

$$\overline{w} = \frac{100E_2}{q_0 h^4 S^2} w,\ \left(\overline{\sigma}_{xx}, \overline{\sigma}_{yy}, \overline{\tau}_{xy}\right) = \frac{E_2}{q_0 S^2}\left(\sigma_{xx}, \sigma_{yy}, \tau_{xy}\right),\ \overline{\tau}_{xz} = \frac{1}{q_0 S}\tau_{xz}. \tag{59}$$

where S = a/h.

This normalization ensures a consistent assessment of the influence of the a/b and a/h ratios on the plate response and allows for direct comparison with reference results.

The results presented in Table 6 show agreement with reference solutions based on three-dimensional elasticity across the entire range of a/h ratios considered. The deviation in the central deflection remains below approximately 1% for all cases, while the normal stress components σ¯xx and σ¯γγ are reproduced with comparable accuracy, without any noticeable systematic bias.

With increasing a/h, the results approach the asymptotic behavior characteristic of thin plates, and the discrepancies with respect to the reference solutions are further reduced. This trend indicates that the formulation consistently captures the transition between moderately thick and thin plate regimes.

The largest deviations are observed for the transverse shear stress τ¯xz, particularly for lower a/h ratios where shear effects are more pronounced. This behavior is consistent with the known limitations of equivalent single-layer theories, which do not explicitly represent interlaminar discontinuities in shear deformation. Nevertheless, the predicted values remain within the range typically reported for higher-order formulations and accurately reflect the expected level of transverse shear response.

Table 6
Normalized central deflection and stress components for a cross-ply [0/90/90/0] laminated plate under sinusoidal mechanical loading for different a/h ratios.

Model Laminate [0/90/90/0]	a/h	$\overline{w}$	$\overline{\sigma}_{xx}$	$\overline{\sigma}_{yy}$	$\overline{\sigma}_{xy}$	$\overline{\tau}_{xz}$
Present model	4	1.956	0.714	0.650	0.0476	0.246
LW [37]		2.018	0.720	0.692	0.0483	0.229
Elasticity [4]		1.954	0.720	0.666	0.0467	0.270
HSDT [34]		1.886	0.666	0.631	0.0433	0.135
ZigZag [3]		1.893	0.641	0.851	0.0436	0.216
LW [35]		1.978	0.676	0.587	–	0.233
Error (%) vs Elasticity		0.10	0.83	2.40	1.93	8.89
Present model	10	0.737	0.567	0.398	0.0288	0.332
LW [37]		0.759	0.576	0.414	0.0281	0.311
Elasticity [4]		0.743	0.559	0.403	0.0276	0.301
HSDT [34]		0.715	0.547	0.438	0.0267	0.335
ZigZag [3]		0.723	0.546	0.419	0.0269	0.298
LW [35]		0.732	0.543	0.391	0.0281	0.332
Error (%) vs Elasticity		0.81	1.43	1.24	4.35	10.30
Present model	20	0.514	0.547	0.307	0.0240	0.357
LW [37]		0.529	0.561	0.318	0.0237	0.339
Elasticity [4]		0.517	0.543	0.309	0.0230	0.328
HSDT [34]		0.507	0.541	0.365	0.0228	0.382
ZigZag [3]		–	–	–	–	–
LW [35]		–	–	–	–	–
Error (%) vs Elasticity		0.58	0.74	0.65	4.35	8.84
Present model	100	0.435	0.539	0.271	0.0222	0.323
LW [37]		0.448	0.556	0.280	0.0220	0.349
Elasticity [4]		0.435	0.539	0.271	0.0214	0.339
HSDT [34]		0.436	0.541	0.336	0.0215	0.411
ZigZag [3]		0.430	0.537	0.270	0.0212	0.335
LW [35]		0.431	0.543	0.273	–	0.377
Error (%) vs Elasticity		0.02	0.04	0.07	3.74	4.71

The formulation achieves this level of accuracy without introducing

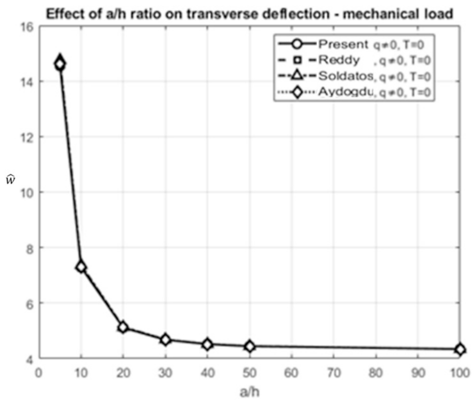

Fig. 3. Effect of the through-thickness shape function on the normalized central deflection of a cross-ply [0/90/90/0] laminate for varying thickness ratios $a/h(a/b = 1)$.

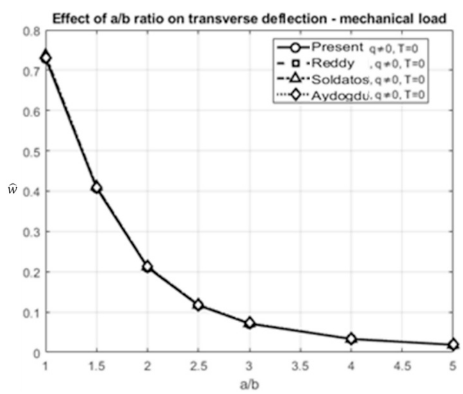

Fig. 4. Effect of the aspect ratio $\frac{a}{b}$ on the normalized central deflection of a cross-ply [0/90/90/0] laminate under mechanical loading ($a/h = 10$).

additional degrees of freedom, thereby avoiding the computational cost associated with layer wise approaches. At the same time, the through-thickness distribution of shear stresses remains smooth and free of numerical oscillations, indicating stable behavior and confirming the suitability of the adopted shape function F(z) for representing transverse shear effects.

Furthermore, the agreement with three-dimensional solutions is maintained even in regimes with pronounced shear contributions, confirming that the formulation captures the dominant mechanisms governing the global response of laminated plates over a wide range of geometric configurations.

Figs. 3 and 4 illustrate the influence of the a/h and a/b ratios on the normalized central deflection of the [0/90/90/0] laminated plate under mechanical loading. The diagrams provide insight into the transition of the dominant deformation mechanisms as a function of the plate geometry, with all considered models exhibiting a very similar global response.

As the a/h ratio increases (Fig. 3), a rapid decrease in deflection is observed for lower values of a/h, followed by a gradual convergence towards an asymptotic limit. This behavior corresponds to the transition from a shear-dominated regime to a bending-dominated response, in which the differences between models become negligible.

A similar trend is observed with increasing a/b (Fig. 4), where the central deflection decreases monotonically and the response stabilizes. For higher aspect ratios, the curves practically coincide, indicating that the structural response is governed primarily by global bending effects, with limited sensitivity to the specific through-thickness kinematic assumptions.

In contrast, for lower values of a/h and a/b, where transverse shear effects are more pronounced, subtle differences between the formulations can be identified. Although these differences remain relatively small, they reflect variations in the representation of through-thickness shear deformation.

Within this context, the proposed formulation exhibits consistent behaviour across the entire range of geometric parameters, without deviations in the transition between shear- and bending-dominated regimes. The smooth and monotonic evolution of the deflection, without spurious oscillations or irregularities, indicates that the adopted shape function F(z) provides a balanced representation of through-thickness kinematics, even in regimes where shear effects are significant.

This behaviour is achieved without introducing additional degrees of freedom, highlighting the efficiency of the formulation relative to more complex approaches.

Figs. 5–9 present the through-thickness distributions of the normalized stress components $\bar{\sigma}_{xx}$, $\bar{\sigma}_{yy}$, $\bar{\tau}_{xy}$, and $\bar{\tau}_{xz}$ in a [0/90/90/0] laminate for different a/h ratios under sinusoidal mechanical loading. These diagrams provide detailed insight into the through-thickness structure of the stress state and its dependence on the plate geometry.

Fig. 5 shows the distribution of normal stress $\bar{\sigma}_{xx}$. Within each layer, stress follows an approximately linear variation, while changes in slope occur at the ply interfaces due to the discrete variation of orthotropic stiffnesses between layers of different orientations. This profile is a direct consequence of the laminated structure and the discontinuity of material properties through the thickness.

The influence of the a/h ratio is primarily reflected in the intensity of these layer wise effects. For lower values of a/h, deviations from an idealized linear profile are observed, indicating a more pronounced contribution of transverse shear deformation. As a/h increases, the distributions gradually approach a globally linear form, and the differences between the curves diminish, corresponding to a transition toward a bending-dominated response.

The stress changes sign at the mid-plane (z/h = 0), while the extreme occurs at the outer surfaces, which is consistent with classical bending behavior.

Fig. 6 presents the distribution of $\bar{\sigma}_{yy}$. In contrast to $\bar{\sigma}_{xx}$, more pronounced slope variations are observed across the interfaces, reflecting the larger differences in effective stiffness in the y-direction between plies of 0° and 90° orientation. As a result, the distribution exhibits a stronger layer wise character and increased sensitivity to interlaminar discontinuities.

The effect of the a/h ratio follows the same qualitative trend as for

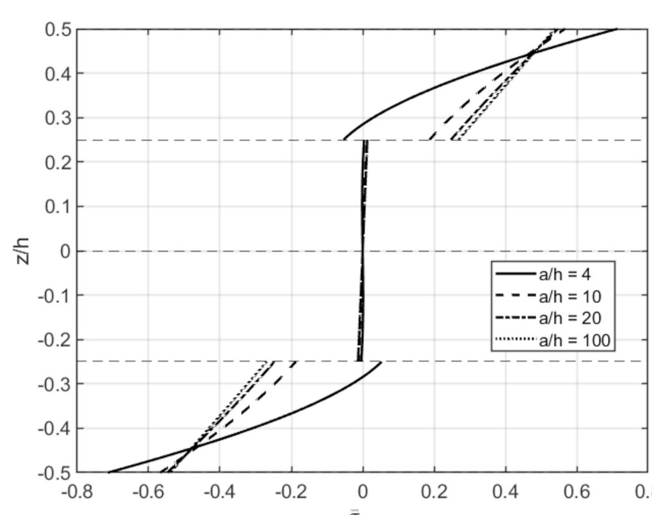

Fig. 5. Through-thickness distribution of the normalized normal stress $\bar{\sigma}_{xx}$ in a [0/90/90/0] laminated plate for different a/h ratios (a/b = 1).

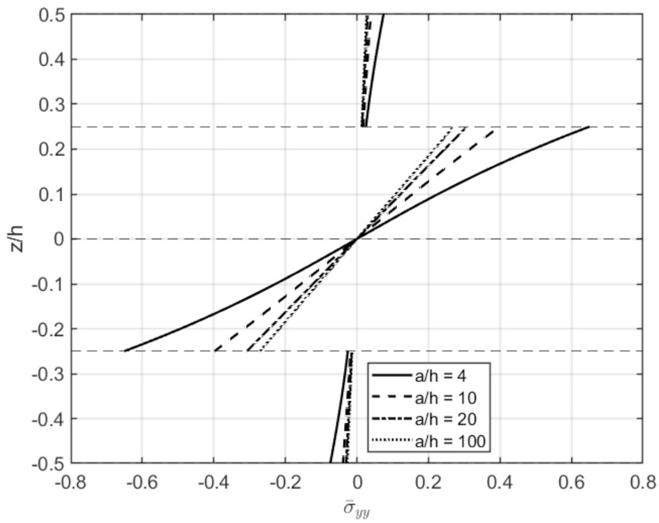

Fig. 6. Through-thickness distribution of the normalized normal stress $\bar{\sigma}_{\gamma\gamma}$ in a [0/90/90/0] laminated plate for different a/h ratios (a/b = 1).

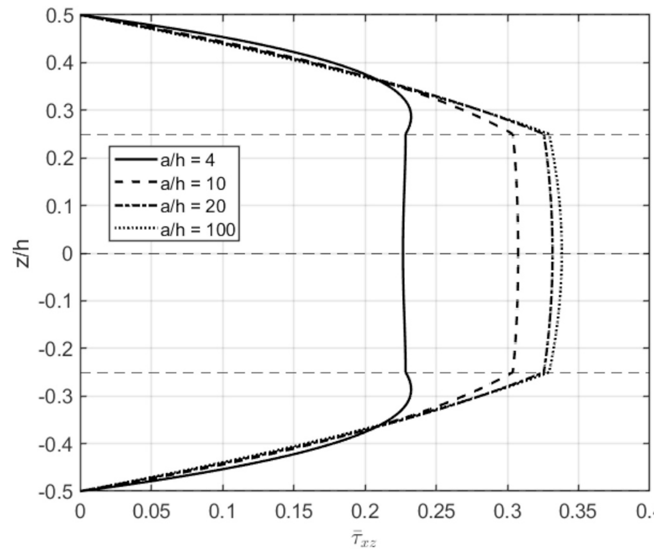

Fig. 8. Through-thickness distribution of the normalized transverse shear stress $\bar{\tau}_{x}z$ in a [0/90/90/0] laminated plate for different a/h ratios (a/b = 1).

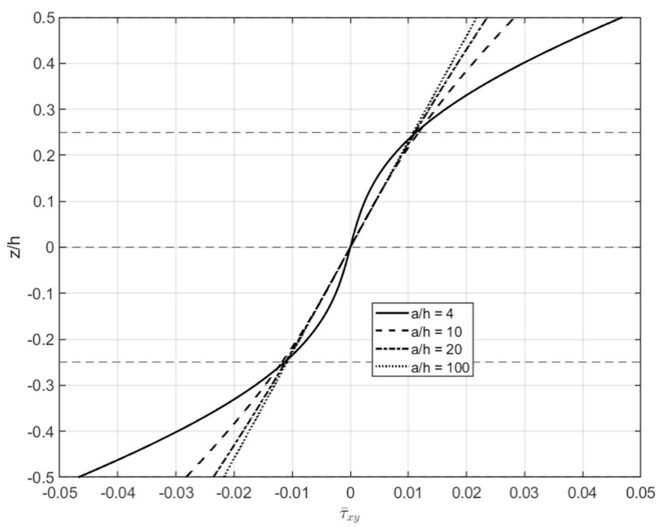

Fig. 7. Through-thickness distribution of the normalized in-plane shear stress $\bar{\tau}_{x\gamma}$ in a [0/90/90/0] laminated plate for different a/h ratios (a/b = 1).

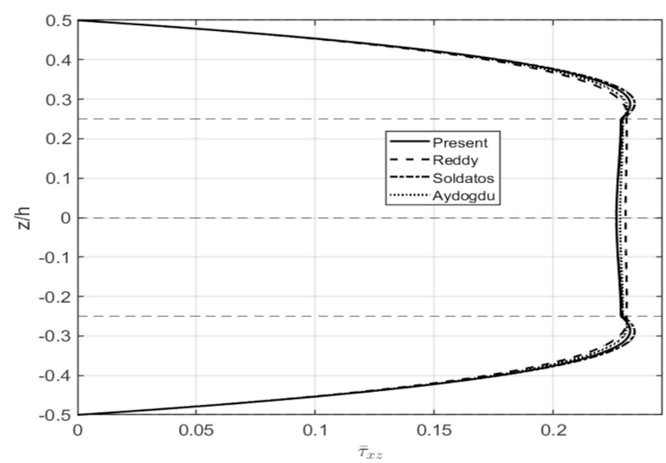

Fig. 9. Comparison of through-thickness distributions of the normalized transverse shear stress $\bar{\tau}_{x}z$ in a [0/90/90/0] laminated plate for different through-thickness shape functions (a/h = 4, a/b = 1).

$\bar{\sigma}_{xx}$: for lower values of a/h, more noticeable deviations from linearity are present, while with increasing a/h the distributions tend toward a linear profile and the curves converge. The location of characteristic points remains unchanged, and the distribution retains its anti-symmetric character with respect to the mid-plane.

Overall, the results confirm that the formulation consistently reproduces the through-thickness structure of normal stresses in laminated composites, while accurately capturing the influence of material anisotropy and geometric parameters.

Fig. 7 shows the through-thickness distribution of the normalized in-plane shear stress $\bar{\tau}_{x\gamma}$ in a [0/90/90/0] laminate for different a/h ratios under sinusoidal mechanical loading. The distribution exhibits an anti-symmetric profile with respect to the mid-plane (z/h = 0), where the stress changes sign.

Unlike the normal stress components, $\bar{\tau}_{x\gamma}$ remains continuous across the entire thickness, without slope discontinuity at the ply interfaces. This behavior indicates that the in-plane shear response is governed predominantly by the global deformation field, with limited sensitivity to the discrete variation of material properties through the thickness.

The effect of the a/h ratio is reflected in the curvature of the distribution: for lower values of a/h, a more pronounced nonlinearity is observed near the mid-plane, while with increasing a/h the profile approaches a linear variation and the differences between the curves diminish. This trend is consistent with the transition toward a bending-dominated regime.

Fig. 8 presents the distribution of the normalized transverse shear stress $\bar{\tau}_{x}z$, which is particularly sensitive to the adopted through-thickness kinematics. The obtained profiles exhibit a nonlinear variation, with zero values at the free surfaces (z/h = ±0.5) and maxima within the laminate thickness, consistent with the requirements of transverse shear equilibrium and traction-free boundary conditions.

In contrast to the in-plane shear component, $\bar{\tau}_{x}z$ is directly governed by the through-thickness kinematic description. The predicted distributions remain smooth and free of spurious oscillations across the entire thickness, indicating a stable representation of transverse shear deformation.

The influence of the a/h ratio is observed through changes in the curvature and intensity of the distribution: for lower a/h values, where shear effects are more pronounced, stronger nonlinearity is present, while with increasing a/h the profiles become smoother and tend toward a parabolic shape. The differences between the curves simultaneously decrease, reflecting the reduced significance of transverse shear in thin plate regimes.

This behavior indicates that the proposed formulation captures the transverse shear response in a manner consistent with three-dimensional elasticity, without introducing additional degrees of freedom.

Fig. 9 presents a comparison of the through-thickness distribution of the normalized transverse shear stress τ¯xz in a [0/90/90/0] laminate obtained using different formulations under sinusoidal mechanical loading.

All considered models reproduce the same qualitative distribution, characterized by zero values at the free surfaces (z/h = ±0.5) and maximum values within the laminate thickness, consistent with equilibrium requirements and boundary conditions.

The results obtained using the present formulation show an almost complete agreement with the reference solutions, with differences confined to narrow regions near the maximum values and transition zones. These discrepancies are small and do not affect the overall shape of the distribution or the location of characteristic points.

It is particularly important that the proposed model yields a smooth distribution without numerical oscillations, indicating a stable representation of transverse shear behavior. In contrast to some formulations where local irregularities may appear near the peak regions, such effects are not observed here.

The obtained results confirm that the proposed shape function F(z) provides a consistent representation of transverse shear stresses in agreement with three-dimensional elasticity, while retaining a reduced kinematic complexity.

4.4. Thermo-mechanical loading

To further assess the capability of the proposed formulation to capture coupled effects, the bending response of a symmetric [0/90/90/0] laminated plate subjected to combined sinusoidal mechanical loading and thermal loading (type I) is considered. This configuration represents a more demanding problem compared to the previously analyzed cases, as it involves the simultaneous interaction of mechanically and thermally induced deformation mechanisms.

The mechanical load is applied in sinusoidal form, while the temperature field follows a type I distribution, introducing an antisymmetric variation of thermal strains through the thickness. As a result, bending is generated even in the absence of external mechanical loading.

When combined, these loading conditions lead to a coupled thermo-mechanical response in which bending and shear effects of different origins interact, producing a complex stress and deformation state.

This loading configuration enables a direct evaluation of the formulation's ability to consistently capture coupled thermo-mechanical behavior while preserving an accurate through-thickness representation of stresses and deformations.

Within the adopted linear formulation, the overall response of the laminate can be represented as the superposition of the mechanical and thermal contributions. This property is numerically verified through the agreement between the directly computed combined solution and the sum of the independently obtained mechanical and thermal deflections.

Accordingly, the dimensionless deflection is defined using separate normalizations for the mechanical and thermal components:

$$\overline{w}_{\text{mech}} = \frac{10^3 w_{\text{mech}}}{q_0 a^4/(E_2 h^3)}, \; \overline{w}_{\text{therm}} = \frac{10 h w_{\text{therm}}}{\alpha_1 T_1 a^2} \tag{60}$$

while the combined response is expressed as

$$\overline{w}_{\text{comb}} = \overline{w}_{\text{mech}} + \overline{w}_{\text{therm}} \tag{61}$$

This decomposition enables a direct quantification of the relative contributions of mechanical and thermal loading to the overall laminate response.

The results presented in Table 7. clearly demonstrate a fundamentally different scaling behavior of the mechanical and thermal contributions with respect to the thickness ratio a/h. Although both components decrease with increasing slenderness, their sensitivity to this parameter is markedly non-uniform.

Table 7
Influence of the through-thickness shape function on the normalized central deflection of a cross-ply [0/90/90/0] laminate under sinusoidal thermo-mechanical loading (a/b = 1).

a/h	Model	$\overline{w}_{\text{comb}}$	$\overline{w}_{\text{therm}}$	$\overline{w}_{\text{mech}}$
5	Present	15.6177	1.0720	14.5456
	Reddy [10]	15.4080	1.0709	14.3371
	Soldatos [15]	15.6309	1.0721	14.5588
	Aydogdu [16]	15.5372	1.0716	14.4656
10	Present	8.3329	1.0463	7.2866
	Reddy [10]	8.2495	1.0459	7.2036
	Soldatos [15]	8.3363	1.0462	7.2900
	Aydogdu [16]	8.3000	1.0462	7.2538
20	Present	6.1381	1.0355	5.1026
	Reddy [10]	6.1133	1.0354	5.0779
	Soldatos [15]	6.1390	1.0355	5.1035
	Aydogdu [16]	6.1283	1.0355	5.0928
30	Present	5.7012	1.0332	4.6680
	Reddy [10]	5.6897	1.0331	4.6566
	Soldatos [15]	5.7016	1.0332	4.6684
	Aydogdu [16]	5.6966	1.0331	4.6635
40	Present	5.5457	1.0323	4.5134
	Reddy [10]	5.5392	1.0323	4.5069
	Soldatos [15]	5.5459	1.0323	4.5136
	Aydogdu [16]	5.5431	1.0323	4.5108
50	Present	5.4731	1.0319	4.4412
	Reddy [10]	5.4689	1.0319	4.4370
	Soldatos [15]	5.4732	1.0319	4.4414
	Aydogdu [16]	5.4714	1.0319	4.4395

The mechanical contribution $\overline{w}_{\text{mech}}$ undergoes a pronounced reduction as a/h increases, which is consistent with the progressive suppression of transverse shear effects in slender configurations. In contrast, the thermal contribution $\overline{w}_{\text{therm}}$ exhibits only a weak dependence on a/h, indicating that its magnitude is predominantly governed by through-thickness thermal gradients rather than kinematic constraints associated with plate thickness. As a result, the relative participation of the thermal component in the total response increases with increasing a/h, despite a slight decrease in its absolute value.

A comparative assessment of different through-thickness shape functions reveals that discrepancies are primarily confined to the lower a/h range, where shear deformation remains significant. In this regime, variations in the combined response $\overline{w}_{\text{comb}}$ remain within approximately 1–2% and are predominantly driven by differences in the mechanical contribution, while the thermal response remains largely insensitive to the assumed kinematic description.

With increasing a/h, all formulations exhibit rapid convergence, reflecting the transition toward a bending-dominated regime in which the influence of higher-order kinematic assumptions becomes negligible. This asymptotic consistency not only validates the robustness of the formulation but also confirms its capability to provide stable and reliable predictions across a wide range of thickness ratios.

The proposed formulation (Present), in the regime of lower (a/h) ratios where transverse shear effects are dominant, yields result that remain within the range of reference higher-order theories, without altering the global response trend. As (a/h) ratio increases, the predicted values converge toward those obtained by other formulations, confirming that the adopted shape function ensures a consistent transition between thick and thin laminate regimes.

This behavior indicates that the proposed shape function provides a stable and physically consistent representation of the coupled thermo-mechanical response, particularly in the regime where shear deformation is most pronounced, without the need for additional degrees of freedom.

Fig. 10 shows that the combined response retains the same functional

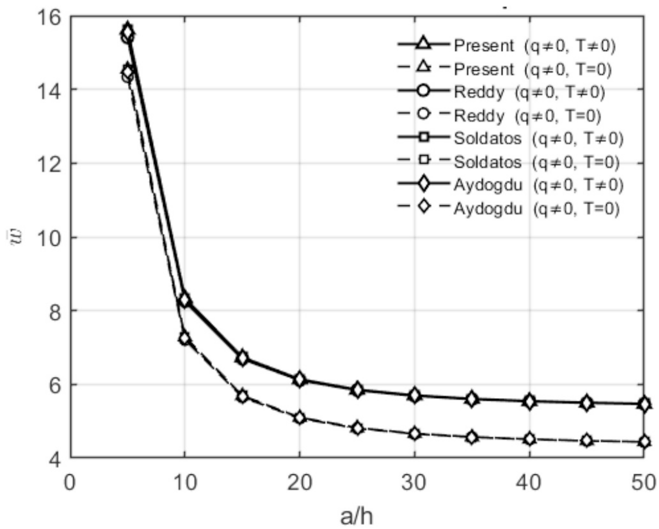

Fig. 10. Comparison of the normalized combined and mechanical central deflections as a function of the a/h ratio for a [0/90/90/0] laminate under sinusoidal thermo-mechanical loading (a/b = 1).

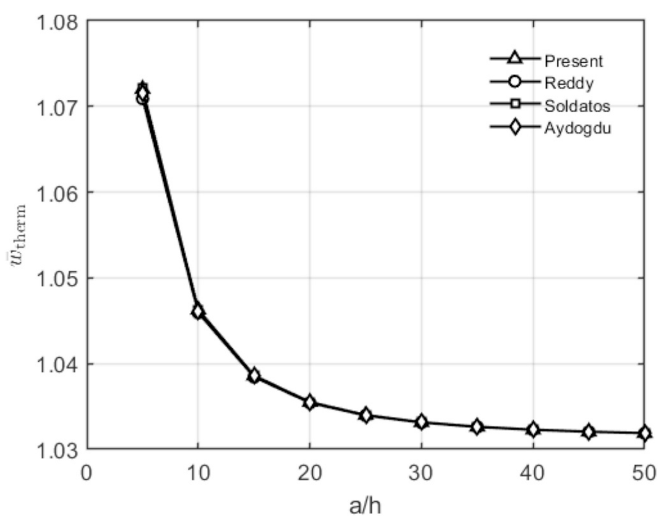

Fig. 11. Influence of the through-thickness shape function on the normalized thermal deflection as a function of the a/h ratio for a [0/90/90/0] laminate under sinusoidal thermal loading (a/b = 1).

dependence on the (a/h) ratio as the mechanical component, with the difference between the curves appearing as an almost constant offset along the vertical axis due to the additional thermal contribution. This indicates that, in the present case, the thermal effect acts primarily as an additive component, without altering the underlying deformation mechanism. The proposed shape function (Present) consistently follows the behavior of the reference formulations across the entire range, remaining within a narrow band of values in the lower (a/h) regime where shear effects are most pronounced, without exhibiting any local deviations. As plate slenderness increases, the differences between the models diminish, and all formulations converge toward the same asymptotic behavior.

Fig. 11 presents the thermal contribution to the deflection, where a monotonic decrease of $\overline{w}_{\mathrm{therm}}$ with increasing (a/h) is observed, within a relatively limited range of variation. The predicted curves show an almost complete overlap for all considered shape functions, indicating that the thermal component of the response is governed predominantly by the imposed temperature field, with negligible sensitivity to the assumed through-thickness kinematics.

When considered together with the results in Table 7, these observations indicate that the influence of the through-thickness shape function manifests primarily through the mechanical component of the response, while the thermal contribution remains largely unaffected. The proposed formulation provides consistent agreement with the reference models across the entire range of (a/h), including the shear-dominated regime, as well as complete convergence in the asymptotic limit of thin plates.

This behavior confirms that the adopted shape function enables a stable and physically consistent representation of the coupled thermo-mechanical response, maintaining accuracy in regimes where transverse shear effects are dominant, without requiring additional layer wise enhancements or increased kinematic complexity.

5. Conclusion

A finite element formulation based on an ESL–HSDT framework has been developed, in which the through-thickness shape function is defined variationally in an exponential form. This approach establishes a direct link between the assumed kinematics and the distribution of transverse shear energy, thereby eliminating the arbitrariness inherent in predefined thickness functions.

The proposed model demonstrates consistent accuracy across a broad range of benchmark problems, including orthotropic and laminated plates subjected to mechanical, thermal, and coupled thermo-mechanical loading. The agreement is particularly strong for global response quantities, while larger deviations observed for local transverse shear stresses remain consistent with the known limitations of ESL formulations.The agreement with reference solutions is achieved not only for global response quantities, but also in regimes where transverse shear effects are dominant, confirming that the formulation accurately captures the governing deformation mechanisms without loss of stability and without the need for shear correction factors.

A key outcome of the study is the clear separation between mechanical and thermal contributions to the overall response. While the mechanical component governs the scaling and evolution of deflection with respect to plate slenderness, the thermal contribution is primarily dictated by the imposed temperature field and exhibits limited sensitivity to the adopted kinematic assumptions. In the coupled response, this manifests as an additive thermal contribution that preserves the functional form of the mechanical solution, enabling a direct interpretation of their interaction.

The formulation provides a stable and physically consistent representation of transverse shear stresses, characterized by smooth through-thickness distributions, absence of spurious oscillations, and correct satisfaction of boundary conditions. This behavior is particularly evident in shear-dominated regimes and under spatially varying loading, where the influence of the through-thickness kinematics is most pronounced.

The achieved level of accuracy is obtained within a C^0 finite element framework with a limited number of degrees of freedom. In this way, increased computational complexity is avoided, while maintaining a physically consistent representation of transverse shear effects within an equivalent single-layer formulation.

Overall, the results confirm that the proposed formulation constitutes a robust and physically grounded approach for the analysis of laminated composite plates under coupled thermo-mechanical loading, in which the variationally defined shape function plays a central role in ensuring consistent and reliable predictions across a wide range of geometric parameters.

CRediT authorship contribution statement

Aleksandar Radaković: Writing – original draft, Validation, Software, Methodology, Formal analysis, Conceptualization. **Dragan Čukanović:** Visualization, Validation, Investigation, Formal analysis.

Gordana Bogdanović: Supervision, Methodology, Conceptualization. **Petar Knežević:** Writing – review & editing, Methodology, Data curation. **Strahinja Milenković:** Validation, Investigation, Data curation. **Aleksandar Nešović:** Visualization, Investigation, Formal analysis.

Declaration of competing interest

The authors declare that they have no known competing financial interests or personal relationships that could have appeared to influence the work reported in this paper.

Data availability

Data will be made available on request.

References

[1] Tungikar VB, Rao KM. Three dimensional exact solution of thermal stresses in rectangular composite laminate. Compos Struct 1994;27:419–30. https://doi.org/10.1016/0263-8223(94)90268-2.

[2] Joshan YS, Grover N, Singh BN. Analytical modelling for thermo-mechanical analysis of cross-ply and angle-ply laminated composite plates. Aerosp Sci Technol 2017;70:137–51. https://doi.org/10.1016/j.ast.2017.07.041.

[3] Shariyat M. Thermal buckling analysis of rectangular composite plates with temperature-dependent properties based on a layerwise theory. Thin-Walled Struct 2007;45:439–52. https://doi.org/10.1016/j.tws.2007.03.004.

[4] Pagano NJ. Exact Solutions for Rectangular Bidirectional Composites and Sandwich Plates. J Compos Mater 1970;4:20–34. https://doi.org/10.1177/002199837000400102.

[5] Noor AK, Kim YH, Peters JM. Transverse shear stresses and their sensitivity coefficients in multilayered composite panels. AIAA J 1994;32:1259–69. https://doi.org/10.2514/3.12128.

[6] Reissner E. The Effect of Transverse Shear Deformation on the Bending of Elastic Plates. J Appl Mech 1945;12:A69–77. https://doi.org/10.1115/1.4009435.

[7] Mindlin RD. Influence of Rotatory Inertia and Shear on Flexural Motions of Isotropic. Elastic Plates. J Appl Mech 1951;18:31–8. https://doi.org/10.1115/1.4010217.

[8] Pai PF. A new look at shear correction factors and warping functions of anisotropic laminates. Int J Solids Struct 1995;32:2295–313. https://doi.org/10.1016/0020-7683(94)00258-X.

[9] Reddy JN. Mechanics of Laminated Composite Plates and Shells. 0 ed. CRC Press; 2003. doi: 10.1201/b12409.

[10] Reddy JN. A Simple Higher-Order Theory for Laminated Composite Plates. J Appl Mech 1984;51:745–52. https://doi.org/10.1115/1.3167719.

[11] Reddy JN. A Review of Refined Theories of Laminated Composite Plates. Shock Vib Dig 1990;22:3–17. https://doi.org/10.1177/058310249002200703.

[12] Reddy JN, Robbins DH. Theories and Computational Models for Composite Laminates. Appl Mech Rev 1994;47:147–69. https://doi.org/10.1115/1.3111076.

[13] Carrera E. Theories and finite elements for multilayered, anisotropic, composite plates and shells. ARCO 2002;9:87–140. https://doi.org/10.1007/BF02736649.

[14] Touratier M. An efficient standard plate theory. Int J Eng Sci 1991;29:901–16. https://doi.org/10.1016/0020-7225(91)90165-Y.

[15] Soldatos KP. A transverse shear deformation theory for homogeneous monoclinic plates. Acta Mech 1992;94:195–220. https://doi.org/10.1007/BF01176650.

[16] Aydogdu M. A new shear deformation theory for laminated composite plates. Compos Struct 2009;89:94–101. https://doi.org/10.1016/j.compstruct.2008.07.008.

[17] Grover N, Singh BN, Maiti DK. New Nonpolynomial Shear-Deformation Theories for Structural Behavior of Laminated-Composite and Sandwich Plates. AIAA J 2013;51:1861–71. https://doi.org/10.2514/1.J052399.

[18] Mantari JL, Bonilla EM, Guedes SC. A new tangential-exponential higher order shear deformation theory for advanced composite plates. Compos Part B Eng 2014;60:319–28. https://doi.org/10.1016/j.compositesb.2013.12.001.

[19] Tounsi A, Houari MSA, Benyoucef S, Adda Bedia EA. A refined trigonometric shear deformation theory for thermoelastic bending of functionally graded sandwich plates. AST 2013;24:209–20. https://doi.org/10.1016/j.ast.2011.11.009.

[20] Mantari JL, Granados EV. Thermoelastic analysis of advanced sandwich plates based on a new quasi-3D hybrid type HSDT with 5 unknowns. Compos Part B Eng 2015;69:317–34. https://doi.org/10.1016/j.compositesb.2014.10.009.

[21] El Meiche N, Tounsi A, Ziane N, Mechab I, Adda. Bedia EA. A new hyperbolic shear deformation theory for buckling and vibration of functionally graded sandwich plate. Int J Mech Sci 2011;53:237–47. https://doi.org/10.1016/j.ijmecsci.2011.01.004.

[22] Sayyad AS, Ghugal YM. A new shear and normal deformation theory for isotropic, transversely isotropic, laminated composite and sandwich plates. Int J Mech Mater Des 2014;10:247–67. https://doi.org/10.1007/s10999-014-9244-3.

[23] Atallah KE, Ouinas D, Zaoui FZ, Khoussa H, Achour B, Hassan MF, et al. A refined quasi-3D higher-order shear deformation theory for static, free vibration, and buckling of laminated composite plates on kerr-type foundation. Next Materials 2025;9:101352. https://doi.org/10.1016/j.nxmate.2025.101352.

[24] Kumar A, Chakrabarti A, Bhargava P. Accurate dynamic response of laminated composites and sandwich shells using higher order zigzag theory. Thin-Walled Structures 2014;77:174–86. https://doi.org/10.1016/j.tws.2013.09.026.

[25] Hauck B, Szekrényes A. Enhanced beam and plate finite elements with shear stress continuity for compressible sandwich structures. Math Mech Solids 2024;29(7):1420–39. https://doi.org/10.1177/10812865231221992.

[26] Zenkour AM, El-Shahrany HD. A simplified four-variable shear deformation theory for advanced composite plates under traction-free surface conditions. Compos Struct 2025;352:119473. https://doi.org/10.1016/j.compstruct.2025.119473.

[27] Reddy JN, Arciniega RA. Shear Deformation Plate and Shell Theories: From Stavsky to Present. Mech Adv Mater Struct 2004;11:535–82. https://doi.org/10.1080/15376490490452777.

[28] Reddy JN. An evaluation of equivalent-single-layer and layerwise theories of composite laminates. Compos Struct 1993;25:21–35. https://doi.org/10.1016/0263-8223(93)90147-I.

[29] Carrera E. An assessment of mixed and classical theories on global and local response of multilayered orthotropic plates. Compos Struct 2000;50:183–98. https://doi.org/10.1016/S0263-8223(00)00099-4.

[30] Zhen W, Kun L. Efficient C0 Finite Element Formulation for Thermal Stress Analysis of Laminated Composite and Sandwich Plates. J Aerosp Eng 2015;28:04014113. https://doi.org/10.1061/(ASCE)AS.1943-5525.0000450.

[31] Sheikh AH, Haldar S, Sengupta D. A high precision shear deformable element for the analysis of laminated composite plates of different shapes. Compos Struct 2002;55:329–36. https://doi.org/10.1016/S0263-8223(01)00149-0.

[32] Sheikh AH, Chakrabarti A. A new plate bending element based on higher-order shear deformation theory for the analysis of composite plates. Finite Elem Anal Des 2003;39:883–903. https://doi.org/10.1016/S0168-874X(02)00137-3.

[33] Khoa NN, Thinh TI. Finite element analysis of laminated composite plates using high order shear deformation theory. Vietnam Journal of Mechanics 2007;29:47–57. https://doi.org/10.15625/0866-7136/29/1/5590.

[34] Ferreira AJM. A formulation of the multiquadric radial basis function method for the analysis of laminated composite plates. Compos Struct 2003;59:385–92. https://doi.org/10.1016/S0263-8223(02)00239-8.

[35] Ganapathi M, Patel BP, Makhecha DP. Nonlinear dynamic analysis of thick composite/sandwich laminates using an accurate higher-order theory. Composite Structures Part B: Engineering 2004;35:345–55. https://doi.org/10.1016/S1359-8368(02)00075-6.

[36] Ye W, Gan L, Liu J, Wang P, Ji C, Chen L, et al. Novel 3D semi-analytical formulation via SBFEM for thermal stress and buckling analyses of laminated plates with 2D discretization. Compos Struct 2026;382:120055. https://doi.org/10.1016/j.compstruct.2026.120055.

[37] Cetkovic M. Thermo-mechanical bending of laminated composite and sandwich plates using layerwise displacement model. Compos Struct 2015;125:388–99. https://doi.org/10.1016/j.compstruct.2015.01.051.

[38] Roque CMC, Ferreira AJM, Jorge RMN. Modelling of composite and sandwich plates by a trigonometric layerwise deformation theory and radial basis functions. Composite Structures Part B: Engineering 2005;36:559–72. https://doi.org/10.1016/j.compositesb.2005.05.003.

[39] Savoia M, Reddy JN. A Variational Approach to Three-Dimensional Elasticity Solutions of Laminated Composite Plates. J Appl Mech 1992;59:S166–75. https://doi.org/10.1115/1.2899483.

[40] Carrera E. Developments, ideas, and evaluations based upon Reissner's Mixed Variational Theorem in the modeling of multilayered plates and shells. Appl Mech Rev 2001;54:301–29. https://doi.org/10.1115/1.1385512.

[41] Cho M, Parmerter RR. Efficient higher order composite plate theory for general lamination configurations. AIAA J 1993;31:1299–306. https://doi.org/10.2514/3.11767.

[42] Kant T, Swaminathan K. Analytical solutions for free vibration of laminated composite and sandwich plates based on a higher-order refined theory. Compos Struct 2001;53:73–85. https://doi.org/10.1016/S0263-8223(01)00019-8.

[43] Zenkour AM. Thermal buckling of functionally graded plates with various boundary conditions according to a refined trigonometric plate theory. Compos Struct 2024;330:117823. https://doi.org/10.1016/j.compstruct.2023.117823.

[44] Samaniego E, Anitescu C, Goswami S, Nguyen-Thanh VM, Guo H, Hamdia K, et al. An energy approach to the solution of partial differential equations in computational mechanics via machine learning: Concepts, pitfalls and improving effects. Comput Methods Appl Mech Eng 2020;362:112790.

[45] Goswami S, Anitescu C, Rabczuk T. VINO: Variational Neural Operator for solving boundary value problems. Comput Methods Appl Mech Eng 2025;437:117785.

[46] Bathe KJ. Finite Element Procedures. 2nd ed. Watertown, MA: Klaus-Jürgen Bathe; 2014.

[47] Dvorkin EN, Bathe KJ. A continuum mechanics based four-node shell element for general nonlinear analysis. Eng Comput 1984;1:77–88. https://doi.org/10.1108/eb023562.